The Pre-Depression Investigation of Cloud Systems in the Tropics (PREDICT) Experiment: Scientific Basis, New Analysis Tools and Some First Results

Michael T. Montgomery[1,2], Christopher Davis[3], Timothy Dunkerton[4,1], Zhuo Wang[5], Christopher Velden[6], Ryan Torn[7], Sharanya J. Majumdar[8], Fuqing Zhang[9], Roger K. Smith[10], Lance Bosart[7], Michael M. Bell[1,2], Jennifer S. Haase[11], Andrew Heymsfield[3], Jorgen Jensen[3], Teresa Campos[3] and Mark A. Boothe[1]

[1]Department of Meteorology, Naval Postgraduate School, Monterey, CA

[2]NOAA's Hurricane Research Division, Miami, FL

[3]National Center for Atmospheric Research, Boulder, CO[!]

[4]Northwest Research Associates, Bellevue, WA

[5]Department of Atmospheric Sciences, University of Illinois at Urbana-Champaign, Urbana, IL

[6]University of Wisconsin/CIMSS, Madison, WI

[7]Department of Atmospheric and Environmental Sciences, University at Albany, State University of New York, Albany, NY

Report Documentation Page

1. REPORT DATE **2011**	2. REPORT TYPE	3. DATES COVERED **00-00-2011 to 00-00-2011**

4. TITLE AND SUBTITLE	
The Pre-Depression Investigation of Cloud Systems in the Tropics (PREDICT) Experiment: Scientific Basis, New Analysis Tools and Some First Results	5a. CONTRACT NUMBER
	5b. GRANT NUMBER
	5c. PROGRAM ELEMENT NUMBER
6. AUTHOR(S)	5d. PROJECT NUMBER
	5e. TASK NUMBER
	5f. WORK UNIT NUMBER
7. PERFORMING ORGANIZATION NAME(S) AND ADDRESS(ES) **Naval Postgraduate School,Department of Meteorology,Monterey,CA,93943**	8. PERFORMING ORGANIZATION REPORT NUMBER
9. SPONSORING/MONITORING AGENCY NAME(S) AND ADDRESS(ES)	10. SPONSOR/MONITOR'S ACRONYM(S)
	11. SPONSOR/MONITOR'S REPORT NUMBER(S)

12. DISTRIBUTION/AVAILABILITY STATEMENT
Approved for public release; distribution unlimited

13. SUPPLEMENTARY NOTES
Bulletin of the American Meteorological Society, Accepted with minor revision: 2011

14. ABSTRACT

The principal hypotheses of a new model of tropical cyclogenesis, known as the marsupial paradigm, were tested in the context of Atlantic tropical disturbances during the National Science Foundation-sponsored Pre-Depression Investigation of Cloudsystems in the Tropics (PREDICT) experiment in 2010. PREDICT was part of a triagency collaboration, with the National Aeronautics and Space Administration?s Genesis and Rapid Intensification Processes (NASA GRIP) experiment and the National Oceanic and Atmospheric Administration?s Intensity Forecasting Experiment (NOAA IFEX), intended to examine both developing and non-developing tropical disturbances. During PREDICT, a total of 26 missions were flown with the NSF/NCAR GV aircraft sampling eight tropical disturbances. Among these were four cases (Fiona, ex-Gaston, Karl and Matthew) for which three or more missions were conducted, many on consecutive days. Because of the scientific focus on the Lagrangian nature of the tropical cyclogenesis process, a wave-relative frame of reference was adopted throughout the experiment in which various model- and satellite-based products were examined to guide aircraft planning and real-time operations. Here, the scientific products and examples of data collected are highlighted for several of the disturbances. The suite of cases observed represent arguably the most comprehensive, self-consistent dataset ever collected on the environment and mesoscale structure of developing and nondeveloping pre-depression disturbances.

15. SUBJECT TERMS

16. SECURITY CLASSIFICATION OF:			17. LIMITATION OF ABSTRACT	18. NUMBER OF PAGES	19a. NAME OF RESPONSIBLE PERSON
a. REPORT **unclassified**	b. ABSTRACT **unclassified**	c. THIS PAGE **unclassified**	**Same as Report (SAR)**	**60**	

[8]Rosenstiel School of Marine and Atmospheric Science, University of Miami,

Miami, FL

[9]Department of Meteorology, Pennsylvania State University,

University Park, PA

[10]Meteorological Institute, Ludwig-Maximilians University, Munich, Germany

[11]Department of Earth and Atmospheric Sciences, Purdue University

West Lafayette, IN

Abstract

The principal hypotheses of a new model of tropical cyclogenesis, known as the marsupial paradigm, were tested in the context of Atlantic tropical disturbances during the National Science Foundation-sponsored *Pre-Depression Investigation of Cloud-systems in the Tropics* (PREDICT) experiment in 2010. PREDICT was part of a tri-agency collaboration, with the National Aeronautics and Space Administration's *Genesis and Rapid Intensification Processes* (NASA GRIP) experiment and the National Oceanic and Atmospheric Administration's *Intensity Forecasting Experiment* (NOAA IFEX), intended to examine both developing and non-developing tropical disturbances.

During PREDICT, a total of 26 missions were flown with the NSF/NCAR GV aircraft sampling eight tropical disturbances. Among these were four cases (Fiona, ex-Gaston, Karl and Matthew) for which three or more missions were conducted, many on consecutive days. Because of the scientific focus on the Lagrangian nature of the tropical cyclogenesis process, a wave-relative frame of reference was adopted throughout the experiment in which various model- and satellite-based products were examined to guide aircraft planning and real-time operations. Here, the scientific products and examples of data collected are highlighted for several of the disturbances. The suite of cases observed represent arguably the most comprehensive, self-consistent dataset ever collected on the environment and mesoscale structure of developing and non-developing pre-depression disturbances.

1. Introduction

A longstanding challenge for hurricane forecasters, theoreticians and numerical weather forecast systems is to distinguish tropical waves that will develop into hurricanes from tropical waves that will not. While tropical easterly waves occur frequently over the Atlantic and East Pacific, only a small fraction of these waves (~20%; e.g., Frank 1970) evolve into tropical storms when averaged over the hurricane season. The problem was insightfully summarized by Gray (1998): "*It seems unlikely that the formation of tropical cyclones will be adequately understood until we more thoroughly document the physical differences between those systems which develop into tropical cyclones from those prominent tropical disturbances which have a favorable climatological and synoptic environment, look very much like they will develop but still do not.*"

The formation of tropical cyclones is one of the remaining mysteries of the atmosphere (Emanuel, 2005). As for why it remains unsolved, after decades of research, it is unfortunately true that in-situ observations are lacking over remote tropical oceans. Recent years have seen several field campaigns aimed at understanding the science of tropical cyclone formation. These include the National Aeronautics and Space Administration (NASA) Tropical Cloud Systems and Processes (TCSP) experiment in 2005 (Halverson et al. 2007), the NASA African Multi-Disciplinary Monsoon Analyses (NASA-AMMA) project in 2006 (Zipser et al. 2009), and the Tropical Cyclone Structure experiment in 2008 (TCS-08, Elsberry and Harr 2008). Adding the results of earlier efforts such as the Tropical Experiment in Mexico (TEXMEX; Bister and Emanuel 1997, Raymond et al. 1998) and even serendipitous observations of the early intensification of hurricane Ophelia in the Hurricane Rainband and Intensity Change Experiment

(RAINEX, Houze et al. 2006), and occasional observations from reconnaissance aircraft (Reasor et al. 2005), we have a collection of studies that have sampled pieces of a large and complex scientific puzzle. However, with the exception of the TCS08 experiment, the greatest shortcoming of previous campaigns has been the limited in situ observational sampling, both in space and in time. It has been difficult to piece together snapshots of tropical disturbances taken at different times. "Genesis" (defined here as the formation of a tropical depression[1] at sub-synoptic scales) often occurs between sampling times, or after disturbances move out of range.

There are very few in situ observations of both precursors to genesis and the ensuing tropical cyclone formation process. The paucity of observations is aggravated by a lack of *a priori* knowledge of where to sample a candidate disturbance. For a typical African/Atlantic easterly wave, the trough axis extends meridionally over a thousand kilometers or more. The dimension of a tropical storm in this sector is much smaller, a few hundred kilometers. Convective clouds and cloud systems are smaller still. Tropical cyclone formation is intrinsically a multi-scale process (e.g., Gray 1998). The fate of a tropical easterly wave depends on the large-scale environment in which it is embedded, the wave's synoptic structure (e.g., low-level vorticity and middle-level moisture), and convective-scale processes associated with the wave's evolution. The large-scale nec-

---

[1] The glossary on NOAA's Hurricane Research Division's website uses "tropical cyclone as the generic term for a nonfrontal synoptic-scale low-pressure system over tropical or sub-tropical waters with organized convection (i.e. thunderstorm activity) and a definite cyclonic surface wind circulation." Notably, this definition does not invoke any wind threshold. The same glossary defines a "tropical depression" as a tropical cyclone with maximum sustained surface winds of less than 17 $m\,s^{-1}$ (34 kt, 39 mph) and, in the Atlantic and Eastern Pacific Basins, a "tropical storm" as a tropical cyclone with surface winds between $17\,m\,s^{-1}$ and 33 $m\,s^{-1}$. In this study we will define genesis as the formation of a tropical depression and we impose no formal threshold on wind speed.

—

4

essary conditions for tropical cyclone formation have been known for over four decades (e.g., Gray 1968; DeMaria et al. 2001): nonzero cyclonic vorticity in the lower troposphere; sufficiently warm sea surface temperatures (≥ 26 $^\circ$C); a moist middle troposphere; and at most a moderate vertical shear between upper and lower troposphere (no larger than approximately 12 m s^{-1}). Some observational studies have suggested also that the upper-level environmental conditions over a developing low-level disturbance may play an important modulating role (Dvorak 1975; Sadler 1976; McBride and Zehr 1981). Yet, all of these conditions in conjunction are well known to be insufficient.

In late summer 2010 a trio of field campaigns was conducted by the National Aeronautics and Space Administration (NASA), National Oceanic and Atmospheric Administration (NOAA) and National Science Foundation (NSF) to investigate tropical cyclogenesis in the Caribbean and West Atlantic and the subsequent intensification of named storms in these regions. While two of the campaigns[2] included intensification in their portfolio of objectives, the Pre-Depression Investigation of Cloud Systems in the Tropics (PREDICT) campaign was designed exclusively to study genesis. Priority was given to developing storms prior to their classification as tropical depressions even when mature storms were present nearby. The primary measurement platform of PREDICT was the NSF/NCAR GV, equipped with dropsondes and onboard sensors for meteorological variables and ice microphysics, see Table 1. The range and speed of the

---

[2] The Genesis and Rapid Intensification Processes (GRIP) project of the National Aeronautics and Space Administration and the Intensify Forecast Experiment (IFEX) of the National Oceanic and Atmospheric Administration.

GV, and the high altitude (~12-13 km) from which it could release dropsondes, were exploited to sample storm formation from Central America to the mid-Atlantic (roughly 40°W) operating out of St. Croix in the U.S. Virgin Islands (see Figure 1).

The purpose of this article is to present an overview of the scientific basis for PREDICT, a summary of the scientific products used during the experiment and some noteworthy first results that have emerged since the completion of the field phase on 30 September, 2010. An outline of the remaining paper is as follows. A summary of the scientific basis of the experiment and practical impacts is presented in Section 2. Section 3 presents a glimpse of the daily weather briefings and research tools employed to assess candidate tropical disturbances for possible flight operations. Section 4 presents a summary of all of the disturbances flown during the field program and provides some first clues on the development versus non-development issue. Section 5 provides our conclusions about the field phase of this work and sketches a path forward.

2. Scientific Basis and Practical Impacts

In the experiment's conception it was recognized that tropical cyclogenesis is inherently a multi-scale process (Gray 1998) as noted above. What the experiment needed was an overarching framework within which the roles of different scales could be evaluated to determine their relative importance in genesis over the western Atlantic, with presumably strong implications for genesis in other basins. The guiding philosophy for investigation was the following:

Tropical depression formation is greatly favored in the critical-layer region of the synoptic-scale, pre-depression wave or subtropical disturbance.

6

This idea is the underlying tenet of a new model for cyclogenesis in tropical waves developed by Dunkerton et al. (2009, hereafter DMW09), expressed in three hypotheses. In basic fluid dynamical terms, the *cat's eye* recirculation region within the *critical layer* of the parent wave is a region of cyclonic rotation and weak straining deformation (H1). This region provides a set of approximately closed material contours. Inside the cat's eye circulation, air tends to be repeatedly moistened by cumulus convection, protected to some degree from lateral intrusion of dry air and deformation by horizontal or vertical shear, and (thanks to its location near the critical level) able to keep pace with the parent wave until the dominant vortex has strengthened into a self-maintaining entity (H2). During this time the parent wave is maintained and possibly enhanced by diabatically- amplified eddies within the wave (proto-vortices on the mesoscale), a process favored in regions of small intrinsic phase speed (H3). The combination of the associated genesis sequence and the overarching framework for describing how such hybrid wave-vortex structures become tropical depressions/storms is likened to the development of a marsupial infant in its mother's pouch, and for this reason has been charmingly dubbed the "marsupial paradigm". This model is often referred to simply as the "pouch theory".

The new model finds strong support in the four-season observational survey of the Atlantic and eastern Pacific sectors carried out by DMW09, two recent case studies in the Western Pacific sector during the Tropical Cyclone Structure 2008 (TCS08) field experiment (Montgomery et al. 2010a, Raymond and Lopez 2011), the post-analysis of the 2009 PREDICT Dry Run (Wang et al. 2010), and real-case and idealized high-

resolution numerical model simulations (Wang et al. 2010a, b; Montgomery et al. 2010b, Fang and Zhang 2010, 2011). Together, these studies point to the pouch center as the preferred location (or "sweet spot") for cyclogenesis, serving as a "focal point" for an upscale vorticity aggregation process while the wave pouch and proto-vortex move together. As an outgrowth of these basic investigations, a Galilean invariant real-time wave tracking algorithm was developed to predict the possible loci of tropical cyclogenesis within the trough region of westward propagating disturbances (Wang et al. 2009).

Of significance to forecasters is that the wave pouch provides a favorable local environment for the formation and intensification of the tropical cyclone proto-vortex. An immediate consequence of the new model is that the pouch provides a more precise, dynamically relevant target for continuous monitoring that is distinct from the chaotic moist convective activity that is scattered throughout the parent wave's trough. While deep convection outside, or along the edge, of the pouch can be equally vigorous, its longer-term impacts are subject to strain/shear deformation, inimical to development.

To distinguish developing from non-developing waves in the field campaign, and in future studies, we believe that a more complete understanding of the kinematic, dynamic and thermodynamic aspects of the wave's pouch is essential. An improved understanding of the pouch structure has practical benefits as well. Since the sub-synoptic scale wave pouch can be resolved to some extent by coarse-resolution global model analyses and operational data, and predicted several days in advance, a proper diagnosis of the wave pouch can provide useful information to operational forecasters (Wang et al. 2009).

In summary, the main aim of the PREDICT experiment was driven by a basic curiosity for how hurricanes form from tropical waves. A practical outcome of PREDICT will be to provide forecasters with new quantitative metrics for evaluating the prospective development of easterly waves and other disturbances beyond 48 hours.

3. Scientific Tools Used During PREDICT

A. Forecaster Guidance

The forecasting strategy for PREDICT consisted of three components. First, the observed state of the atmosphere was assessed from a "big picture" weather perspective using all available surface and upper air, satellite, and oceanic products, as well as all available numerical model guidance products. Candidate disturbances in the PREDICT domain (Fig. 1) were evaluated using these observational, satellite, and model products over the previous 48 h. Dropsonde observations obtained from the PREDICT GV research aircraft were used to help forecasters anticipate likely changes in convective organization of interest to PREDICT. During the time of peak activity in mid-September there were as many as five candidate disturbances simultaneously over the Atlantic Ocean and adjacent western seas.

After the "big picture" weather perspective was completed and the information assimilated into the forecast process, PREDICT forecasters turned to the available numerical model guidance to evaluate the expected large-scale flow evolution and whether it would be favorable for the development or maintenance of tropical disturbances within the PREDICT domain over the next 120 h with emphasis on 0-72 h. Sharpening the focus on candidate disturbances even further, the pouch products

(http://met.nps.edu/~mtmontgo/storms2010.html) were examined carefully for distur-
bances that exhibited recirculation in a co-moving framework. Forecast model output
was used to quantify the phase velocity of these disturbances in the lower troposphere
over the 120 h forecast period. Typically, the procedure was to analyze the 700-hPa
level. For cases with a pouch initially confined below 700 hPa, the 850 hPa or 925 hPa
levels were used.

Recirculation with a pouch is a necessary but not sufficient condition for devel-
opment. Pouches with an initial value of the 700-hPa Okubo-Weiss parameter of at
least $2 \times 10^{-9} s^{-2}$ that were forecast to grow and/or persist over the 120 h forecast period
became potential targets for GV dropsonde missions to sample pre-genesis and null
disturbances. In simple terms, the Okubo-Weiss (hereafter OW) parameter is a frame-
independent measure of the tendency for a rotational flow to be shape preserving[3].
Mathematically, OW is defined here as $OW = \zeta^2 - S_1^2 - S_2^2 = (V_x - U_y)^2 - (U_x - V_y)^2 - (V_x + U_y)^2$, where S_1 and S_2 denotes strain deformation, ζ denotes vertical vorticity, (U, V) de-
notes zonal and meridional velocity, respectively, and subscripts x and y denote partial
differentiation in the zonal or meridional directions.

In formulating a strategy to determine which pouches should be sampled by air-
craft, the science team needed to recognize that: 1) westward-moving pouches had to

[3] Assuming a scale separation between the slowly varying velocity field and the more rapidly
varying field of squared vorticity (enstrophy), Weiss (1991) and McWilliams (1984) showed that positive
values of OW indicate that the flow is vorticity dominant and shape preserving, whereas negative values
of OW indicate a strain-rate dominated flow susceptible to rapid filamentation. A negative OW region is
unfavorable for rotational organization of deep convection and aggregation of vortical remnants of prior
convective activity.

reach at least 40 W before they would be in range of the GV, 2) disturbances within the PREDICT domain for multiple days would be of greatest interest, and 3) international air-traffic control constraints would limit flight operations in some regions bordering or extending into Haitian, Cuban, Venezuelan or Colombian air space.

The forecast scenarios and strategies were discussed every day during the PREDICT forecast briefings held at 1400 UTC. The findings from this first briefing were shared with PI's from the other agencies at 1500 UTC. This meeting of PI's provided a first opportunity to communicate each group's plan and explore possible avenues of collaboration. A tri-agency call at 1600 UTC, led on a revolving basis by forecasters from each group, provided a forum for all participants to view the day's forecast and flight plans. Similar meteorological information, including the pouch products, was used by all agencies (see companion paper by Evans et al. 2011,submitted to BAMS, for further details).

B. Satellite Products

From basic multispectral imagery, to specialized and experimental products, satellite data (both in digital and graphical form) played multiple important roles in PREDICT pre-mission planning, forecasting, and real-time mission guidance. These data were also used extensively by the GRIP and IFEX project teams and are a valuable asset to ongoing post–field phase analyses. Where available, the GV data will allow crucial in-situ information to assess the accuracy and representativeness of these remotely sensed products and derived fields.

The primary web portal for displaying satellite products and analyses for PRE-DICT was designed by CIMSS and the University of Wisconsin specifically to meet the needs of the field experiment similarly to what has been done for several projects in the past (Hawkins and Velden 2011). In addition to displays of basin-wide imagery with large-scale product overlays, an interactive event-focused window allowed PREDICT analysts and forecasters to hone in on targets with greater detail. Selectable product overlays were available to interrogate the data and subtle mesoscale developments. The site can be found at: http://cimss.ssec.wisc.edu/tropic2/predict. In particular, note the examples in the CIMSS Satellite Blog, put together by a CIMSS graduate student.

In addition to supporting the daily planning and forecasting, tailored satellite products were provided directly to the GV in real time during missions for in-flight analysis on the onboard display system. Hazard avoidance was a top priority of PREDICT flight managers, as the airplane was not designed to fly into highly turbulent regimes. Real-time displays of rapidly-refreshed images of convection and overshooting tops (OTs) along with lightning overlays provided critical support in this regard (for an example of the CIMSS OT product display please see Fig. 2, and also the companion paper for how the product can be useful to PREDICT scientific research). The satellite data included key microwave images (Fig. 3) made available in near real time by the Naval Research Lab group in Monterey via a specialized product collection and dissemination for PREDICT. The displays allowed onboard mission scientists to make crucial decisions on dropsonde locations, augmenting the analysis datasets to better meet the PREDICT science objectives.

To aid real-time guidance, the GOES-EAST satellite was put into rapid-scan operations (RSO) by NOAA/NESDIS on several occasions at the request of PREDICT scientists. The more frequent image scans (every 7 minutes) provided for improved image interpretation of rapidly-developing convection and circulations, and often allowed the pinpointing of smaller-scale circulation centers within the pouch. CIMSS used these images also to derive high-density and coherent atmospheric motion vectors (AMVs) to better define (quantitatively) the sub-synoptic and mesoscale flow features as the pouches evolved (see Fig. 4 for an example). From these winds, analyses of shear and other kinematic variables were derived for use both in real-time analysis and post-experiment case studies (daily examples can be found on the CIMSS PREDICT web page cited above).

As discussed in the foregoing section, the distribution of moisture is a key variable in the new model for genesis: both actively, as a necessary precursor to saturate the column near the pouch center via aggregate convection, and passively, as a tracer to spot entrainment, if any, of dry air into or over the core that can disrupt the genesis process. CIMSS developed a Total Precipitable Water (TPW) product based on morphing microwave sensor data from multiple polar-orbiting platforms (Wimmers and Velden 2007, 2011). An animated, basin-scale product ran continuously during PREDICT and was used every day to assess the large-scale moisture conditions and trends. In addition, an experimental product was developed to show the TPW in a co-moving frame. An example is shown in Figure 5, just a few hours after a GV mission into ex-Gaston

(http://cimss.ssec.wisc.edu/tropic/realtime/tpwROI/ROIs/PGI38L/web/display04W.html, and suggests plausibly how the pouch resists the environmental dry air to the west, and sustains a moist core, at least for 2-3 days in this case. The overlain vectors show the system-relative flow (with the parent wave's phase speed subtracted) of the lower-tropospheric mean wind as deduced from GFS wind analyses. This product illustrates the recirculating flow and trapped moisture in the pouch in the co-moving framework, and will serve as an analysis tool to further assess the new cyclogenesis model.

Another valuable source of moisture analysis is the suite of satellite-derived products to detect the Saharan Air Layer (SAL). This airmass is considered hostile to Atlantic tropical cyclones (Dunion and Velden 2004; Evan et al. 2006; Jones et al. 2007; Wu 2007; Dunion and Marron 2008; Sun et al. 2009; Reale et al. 2009; Shu and Wu 2009), primarily due to the characteristically very dry and dusty mid-level air. Satellite-derived products designed to depict the SAL based on multi-spectral approaches to isolate the dust and dry air effects on radiances are available during the PREDICT period (i.e. the CIMSS main tropical cyclones web site archive). A contentious issue regarding the influence of the SAL on Atlantic TC development is whether the dry air actually gets into the core to disrupt the convection structure. The NOAA/HRD SAL EXperiment (SALEX) missions flown over the past few years are attempting to document this. Certainly, the PREDICT flights will augment this database to provide further information on the SAL-TC interaction.

All of the satellite data and products collected during PREDICT were disseminated to the NCAR EOL field program support facility in Boulder, CO for permanent and free-access archival.

C. `Pouch Products' for GV Flight Planning (Day -1 to -3)

During the field experiment, the sweet spot for TC formation (defined as the intersection of trough axis and critical latitude) derived from global model forecasts was considered as the potential target of research flights. Each day, for each pouch observed at the forecast initial time, a pouch's "vital signs" (see internet link for pouch products given in Sec. A above) and center track were calculated and examined based on the 5-day forecasts from ECMWF, GFS, UKMET, and NOGAPS. A consensus pouch track was formulated also. Operational constraints for most of PREDICT required the depiction of a pouch in the comoving fields (consistent with the marsupial paradigm) of at least one of the global models at analysis time in order to begin tracking a new system (DMW09). By the end of the experiment, however, we were occasionally initiating tracks of vorticity or OW maxima that did not initially exhibit a clear recirculation region in the analysis, but were forecast to do so within a day or so. Each tracked system was assigned a number (beginning at the start of June prior to PREDICT) preceded with the letters 'PGI' which stand for the three projects ongoing during the 2010 Atlantic hurricane season: PREDICT, GRIP and IFEX.

The "pouch tracks" were all plotted atop GOES, TPW, and other diagnostic variables (i.e., 850-hPa relative vorticity, upper-level divergence, etc.) by the CIMSS/U of Wisconsin team. Then a flight pattern was designed based on the pouch track to sample the disturbance over a spatial range of approximately 500 x 500 km centered on the pouch position and over a time period of 4 to 6 hours.

Karl, a well-surveyed case during PREDICT, serves as an illustrative example.

The GV sampled pre-Karl (PGI44) for five consecutive days from 10 -14 September. During the PREDICT mid-day coordination sessions on 13 September, the pouch products based on ECMWF forecasts from 00 UTC 13 September were available for planning the following day's flight. ECMWF 36-hour forecasts depicted a trough located along 82°W at the flight time of 12 UTC 14 September. In the Earth-relative frame, the circulation center as depicted by 700-hPa streamlines was at about 17.3°N and situated on the southern edge of a large region of positive values of the OW parameter (Fig. 6, left). The circulation in the co-moving frame (Fig. 6, right) is better defined than in the earth-relative frame. The 700-hPa earth-relative flow depicts a tropical wave with an inverted-V pattern and only weak westerly flow south of the vortex. The circulation center in the co-moving frame of reference is located between two areas of high OW (Fig. 6, left) that appear to be wrapping around the pouch center. A large lawnmower pattern was constructed that sampled both the earth-relative and co-moving circulations and a region beyond the central convection.

As described during the PREDICT weather briefing at 1400 UTC, 13 September, the CIMSS-PREDICT "invest" page showed that the disturbance was associated with weak deep-layer shear (5-10 kt), a strong lower-tropospheric vorticity maximum embedded in high TPW values, a corridor of high SSTs (29-30 C) along the track of the ECMWF forecast pouch, and convective banding in the VIS/IR satellite imagery. At 21 UTC 14 September, the National Hurricane Center (NHC) declared the disturbance Tropical Storm Karl at (18.3N, 84.2W) (the red dot in Fig. 6). This position is quite close to the forecast sweet spot (18.7N, 83.5W) at the same time (the blue dot in Fig. 6).

D. Ensemble Weather Forecast Products

During the field phase, daily forecast products derived from operational global Ensemble Prediction Systems, experimental regional-scale ensemble analyses and related forecasts augmented short- and long-range planning activities. In future research, these ensemble systems will address hypotheses related to predictability of genesis, the sensitivity of predictions to enhanced observations, and physical insight into the genesis process. For example, the potential development of pre-Karl (PGI44) was identified in the global and mesoscale model ensembles between 5 to 10 days before its officially declared genesis late on 14 September. In the 9-day ECMWF ensemble forecast, the probability of the lower-tropospheric relative vorticity (averaged within a disk of radius 300 km) attaining its verified value at the onset of genesis (5.65×10^{-5} s^{-1}) was still low in the broad region in which Karl was to develop (Fig. 7). In contrast, for the corresponding 7-day forecast initialized two days later, a cluster of solutions of varying strengths, including some consistent with a tropical storm, was evident in the Caribbean (Fig. 7a) with a very different probability distribution (Figs. 7b, c).

For short-range (24-72 h) guidance, two experimental mesoscale ensemble forecast systems were run also during the field phase. The first system was a cycling, mesoscale-ensemble Kalman filter, similar to what is described in Torn (2010) using the Advanced Research WRF model (Skamarock et al. 2005). This system assimilated conventional in situ data, Tropical Cyclone (TC) position and minimum sea-level pressure (SLP), Global Positioning System (GPS) radio-occultation estimates from the Constellation Observing System for Meteorology, Ionosphere, and Climate (COSMIC) array

of satellites (e.g., Anthes et al. 2008), and dropsonde data. A 12-km mesh following any disturbance designated by NHC as an INVEST[5] (or stronger) was nested in a basin-covering 36-km domain. At 0000 UTC and 1200 UTC each day, all 96 ensemble analyses from this system were integrated out 72 hours in order to permit the evaluation of mesoscale probabilistic products and initial condition sensitivity calculations (e.g., Torn and Hakim 2008).

Figure 8 shows the forecast of PGI44 (pre-Karl) at 0000 UTC 14 September initialized at two different times. Whereas the earlier forecast is characterized by larger variance in both the position and minimum SLP, the latter forecast has a tighter probability distribution and is closer to the verification values. The differences in these forecasts likely results from the assimilation of dropsondes from the GV, though further numerical experiments are needed to confirm this. At both initialization times, there is a slight tendency toward the more intense cyclones being farther west.

The other limited-area ensemble prediction system run at the Pennsylvania State University (PSU) was based on a different cycling mesoscale-ensemble Kalman filter (EnKF) (Meng and Zhang 2008a,b; Zhang et al. 2009). The 60-member ensemble system assimilated all non-radiance data used in the NCEP global model on two fixed outer domains centered on St. Croix (with grid spacings of 40.5 and 13.5 km). A vortex- following nest of 4.5 km grid spacing was added for forecasts that were integrated out to 120 h.

---

[5] The term INVEST is used by operational tropical cyclone forecast centers to identify an area of interest for collection of specialized observations or running model guidance. The designation of a system as an INVEST does not correspond to a likelihood of development (NHC, 2010).

Figure 9 shows the track and intensity forecasts of pre-Karl by 8 consecutive sets of forecasts initialized every 12 h from 00Z Sept 10 to 12Z Sept 13. Of the 30 members in each ensemble forecast, the number of members that reached tropical storm strength was 29, 10, 4, 9, 12, 12, 19 and 23 in successive forecasts. Earlier forecasts developed Karl too soon, but this error was reduced in subsequent cycles. Thus, the intensity forecasts in both regional ensemble systems were similar in the case of Karl. The ensemble of tracks maintained a similar spread through time, and were approximately evenly distributed around the observed track of Karl.

4. Tropical Disturbances Observed During PREDICT

The tropical pre-depression environment presented many challenges for research flight operations during PREDICT. The GV is a high performance aircraft that was not designed to penetrate deep convection, but observations were desired in and around the convection within and on the periphery of the pouch. The "square-spiral" flight plan (see Fig. 10) proved to be one of the most successful patterns during the experiment, enabling careful monitoring of developing deep convection as the aircraft spiraled in to the center of the pouch while steadily gaining altitude. Visual, radar, and satellite estimates of convective activity were generally in good agreement, providing confidence that the GV's altitude was high enough to fly above most cloud tops and obtain comprehensive spatial coverage throughout a pre-depression target.

The scientific tools summarized in Section 3 helped the scientists in the operations center devise accurate flight plans and guide the GV safely through a dynamic environment. Updated information about the evolving meteorological situation was avail-

able through a satellite data link, assisting the pilots and mission scientists with in-flight decision-making to improve the quality of the research data collection. Each scientist on board was able to customize their own data displays to focus on the measurements of interest being collected in real-time. Scientists in the operations center were able also to see much of this information and could collaboratively adjust the flight patterns with the flight crew in real-time when necessary.

Apart from the first flight, a test mission on August 15, the remaining 25 PRE-DICT missions examined a variety of disturbances. Figure 11 and Table 2 summarize the systems that were investigated. The nomenclature used to identify disturbances during PREDICT was PGIXX, where XX was the number assigned to a system and retained during its identifiable lifecycle and PGI is an abbreviation for PREDICT-GRIP-IFEX. This number differs from and generally preceded the operational designation by the National Hurricane Center (NHC), whether an INVEST (e.g., 9xL) or tropical depression (e.g., TD1, TD2, etc.). In the case where a storm became a tropical depression or stronger as designated by NHC, it was known by both its PGI number and the official tropical depression number (or storm name).

The storms sampled by PREDICT aircraft missions were fairly evenly split between developing and non-developing systems (see Table 2 for details). While some cases had a high potential for genesis from the time of the first GV flight into them and subsequently developed, one system departed from this pattern. Gaston was a surprising instance where development occurred initially, but following a period of decline (sampled by the GV) re-development did not occur. PGIs 27 and 30 were null cases as anticipated from the time of the first GV mission, but Matthew (PGI46) surprisingly

formed in only three days from a weak disturbance in the mid-Atlantic ITCZ. In the remainder of this section, each of the eight observed disturbances will be summarized along with a few preliminary analyses to assess the non-development of Gaston in comparison with the developing case of Karl.

i. PGI27

PGI27 was first detected near the west coast of Africa on 8 August as a low-amplitude easterly wave. It traversed the tropical Atlantic with a ground-relative speed of 8-9 m s^{-1} westward. Organized deep, moist convection was evident on 16 August and the first flight of the GV was on 17 August. On this flight (RF02) the GV encountered several regions of high ice-water content (IWC). These are of intrinsic scientific interest (e.g. Herman and Heymsfield 2003), and they are also regions of concern for aviation safety. The duration of the most substantial high-IWC penetration was 172 s corresponding to a horizontal path of 40 km, at an altitude of 13 km (Fig. 12). The high-IWC region was penetrated about 2 km below the tropopause at a temperature of about -58°C. At the time of the aircraft penetration, GOES IR imagery showed that this was a region of developing convection with an anvil of about 100 km across (Fig. 12). Ice particle concentration peaked at nearly 10 cm^{-3} (CONCD, 2-50 micron, from a Cloud Droplet Probe, CDP, manufactured by Droplet Measurement Technologies, Boulder, Colorado). As a consequence of the ingestion of high IWC, the temperature sensors filled with ice. The built-in heaters melted part of the ice, and melt-water ran onto the temperature sensor elements, bringing the recorded (total) air temperature to near 0°C (TT_A, from the avionics system). Measurements of ozone concentration show the high

IWC region as characterized by values around 40-50 ppbv, but with peaks > 80 ppbv. These peaks indicate mixing with upper tropospheric and/or stratospheric air. On the following days, PGI27 did not develop; the reasons are not yet clear but may include lack of a well-defined recirculating flow and dry air intrusion.

ii. PGI30

PGI30 was a very weak tropical wave featuring only a tiny area of deep convection (cloud-top temperature of -60°C occupying an area less than 2500 km^2) near the center of a pouch with minimal circulation strength. Convection did persist, episodically, in this region following the wave. Two missions were flown into PGI30, on August 21 and 23, partly to investigate a case that was clearly a non-developer and partly to test the GV dropsonde system, which was experiencing some problems at the time.

iii. Fiona

In contrast to PGI30, pre-Fiona was a strong wave as it moved off the African coast on August 27 at roughly 9 m s^{-1} westward. At the time of the first GV mission on August 30 (centered on about 13 UTC), Fiona was officially still an INVEST (97L), but was upgraded to a tropical storm based on the GV dropsondes (Fig. 10) which indicated a well-organized cyclonic circulation, and based on satellite images showing banded precipitation features (see NHC storm report by Robbie Berg at http://www.nhc.noaa.gov).

Subsequent flights into Fiona occurred on 31 August and 1 September as the storm strengthened slowly but did not reach hurricane intensity. It is hypothesized that

some inhibition of development may have resulted from the vertical shear created by the anticyclonic outflow of hurricane Earl to the northwest of Fiona (Fig. 4). Convection became highly asymmetric, focused on the south (downshear) side of the vortex during this period. Fiona's pouch was subject to Earl's strain deformation as well.

iv. Gaston

Our attention then turned to Gaston, which developed from the African wave following the wave that became Fiona. This system was declared a tropical storm by NHC at 15 UTC 1 September. However, dropsondes from the GV deployed during its first mission into Gaston indicated that the storm had weakened to a tropical depression and Gaston was officially downgraded to an INVEST.

The distribution of moisture was a critical aspect in the evolution of ex-Gaston. Two sources of in situ water vapor profiles were obtained from the GV. The Global Navigation Satellite System Instrument System for Multistatic and Occultation Sensing (GISMOS) was developed for the GV to perform airborne GPS radio occultation (GPS RO) measurements (Garrison et al. 2007; Xie et al. 2008). This measurement technique is based on the same principle as the COSMIC radio occultation profiles used in the WRF ensemble Kalman Filter model mentioned above. GPS RO is a limb-sounding technique that senses the atmosphere using radio signals that traverse the atmosphere as a transmitting GPS satellite sets behind the horizon relative to a moving receiver. The radio wave undergoes refractive bending and a Doppler shift due to variations of refractive index. Retrieval techniques that assume spherical symmetry of the atmosphere map the refractivity variation to the height at the point of closest approach to the

23

Earth, referred to as the tangent point. This horizontal position of the tangent point varies with altitude, hence the vertical refractivity profile is slanted along a horizontal distance of approximately 100-300-km (Fig. 13). Retrievals of water vapor from the observed refractivity are being developed. Future work plans to test the usefulness of these observations in simulating the failure of ex-Gaston to re-develop.

Another perspective on the role of moisture within the pouch of ex-Gaston can be obtained by comparing the thermodynamic structure of ex-Gaston with that of a developing disturbance (pre-Karl to be discussed in more detail below). The day-to-day evolution of the "pouch-mean soundings"[6] obtained from the GV dropsondes during missions into ex-Gaston and the system that finally became Karl are shown in Fig. 14a and Fig. 14b, respectively. These mean pouch soundings are characterized by the virtual potential temperature (θ_v) and pseudo-equivalent potential temperature (θ_e) as a function of height. Features that stand out are:

- There is little difference in the day-to-day variation in θ_v, either in the developing or the nondeveloping system.

- There is a general increase in the lower tropospheric θ_e in both systems, but the increase is not monotonic for Karl.

---

[6] The pouch-mean sounding was derived here provisionally by averaging all soundings of a day's mission with a total precipitable water content larger than 50 kg m^{-2}. This criteria was found to correspond roughly with the region of closed streamline contours at 700 mb in the ECMWF analysis near the time of the mission and eliminated only a small fraction of soundings on the periphery of the system.

- In the nondeveloping system there is a decrease in the mid-tropospheric θ_e, whereas this quantity increases a little in the developing system.

- At the end of the observation period for each disturbance, there is a much larger difference between the near-surface θ_e and the mid-tropospheric θ_e minimum in the non-developing system (~25 K) compared with the difference in the developing system (~17 K).

According to traditional reasoning, the last feature would have implications for the strength of convective downdrafts, which, on the basis of these soundings would be expected to have been larger in the non-developing system (e.g., Emanuel 1994). The argument is that stronger downdrafts (normally attributed to the lower mid-tropospheric relative humidity) would tend to import low θ_e into the boundary layer, offsetting the enhancement of boundary layer θ_e by sea-to-air moisture fluxes. This enhancement is necessary to fuel subsequent deep convective activity. Persistent deep convection is a pre-requisite for genesis through its role in vortex tube stretching and thereby local vorticity generation in the lower troposphere (Montgomery *et al.* 2006, Montgomery and Smith 2010).

A more recent view on the role of mid-level dry air has emerged from numerical simulations using cloud models (James and Markowski 2009, Kilroy 2011, personal communication). These studies suggest that the principal effects of the dry air are to reduce the updraught strength and water loading, while the downdraught strength is not changed appreciably. The reduction of latent heat release leads to a reduction in cloud buoyancy, thereby rendering the clouds less effective in amplifying vertical vorticity. More extensive comparisons of the thermodynamic aspects of developing and nonde-

veloping disturbances in the PREDICT experiment are presented in Smith and Montgomery (2011).

As to the source of this drier air in Gaston, there is evidence of a strong, dry Saharan air mass surrounding the northern hemisphere of Gaston in multiple satellite-derived products (discussed in Section 3B). In addition, dropsonde thermal and moisture profiles do resemble the SAL-type soundings identified in Dunion (2011). However, further analysis is required to determine the contribution of this air mass to the dry air seen in the dropsonde observations.

Dry air continued to plague ex-Gaston during the subsequent days. The cyclonic circulation became shallower over time also. By 5 September, the circulation was not evident at 500 hPa and by 7 September it was barely evident at 700 hPa. The storm continued to produce intense convection intermittently throughout the period, but the vortex systematically weakened.

v. Karl

The pre-Karl disturbance, PGI44 (defined above), originated within the ITCZ region near the northern coast of South America. A surge of southwesterlies over northern South America around 8 September locally strengthened the ITCZ between 50-60°W and resulted in the formation of a quasi-persistent area of convection along the ITCZ near the northern coast of South America. An easterly wave formed subsequently near this locale and propagated westward towards the eastern Caribbean[7]. Convection with-

---

[7] The marsupial framework includes in situ wave formation via hydrodynamic instability of the ITCZ, in addition to neutral wave propagation across the basin (DMW09).

within the early pre-Karl disturbance was elongated east-west on 10 September (Fig. 3). On this day, PREDICT utilized two crews to conduct two missions, one centered on roughly 13 UTC, the other about 6 h later. Both flights revealed a broad gyre of diameter roughly 400 km that featured similar tangential winds between 900 hPa and 500 hPa.

Pre-Karl was rather slow to develop over the next several days. Although not as pronounced as observed in the pouch of Gaston, the minimum θ_e observed in the composite soundings shown in Fig. 14b are believed sufficient to support a pronounced diurnal cycle and boundary layer recovery from 09-13 September with the maximum intensity of convective updrafts (as judged by the CIMSS overshooting top product in Fig. 2)) occurring around 12-15 UTC (late morning local time). Over the course of 11-14 September, convective activity gradually consolidated from an initial southwest-northeast elongation to a more compact pattern encircling the sweet spot within the pouch (Fig. 6), the latter being close to the location where Karl formed later on 14 September. An interesting aspect of Karl is that, despite the large-scale initial circulation, the storm that actually formed was small (Fig. 3).

vi. Matthew

In contrast with Karl, Matthew was generally unforeseen as few as 5 days prior to its formation. While the PREDICT team was tracking weak vorticity features connected with the ITCZ on 17 and 18 September, it was not until deep convection erupted near the analyzed sweet spot on 19 September that there was a feature sufficiently defined in the atmosphere and in global models to plan a mission. The first GV mission was time-centered roughly on 16 UTC September 20. At this time, the pre-Matthew distur-

bance was as weak as PGI27 in terms of the average tangential wind within 300 km of the lower tropospheric circulation center and appeared less organized than Karl at the time of the first mission. However, Matthew quickly organized on 21 and 22 September.

Figure 15 indicates that the pouch was well defined on the 22nd with strong convection occurring close to the predicted maximum in OW and sweet spot in the analysis from the ECMWF model. Matthew went on to develop into a strong tropical storm on 23 September, but despite forecasts of potential rapid intensification, it did not intensify further and made landfall in Belize as a moderate tropical storm late on 24 September. Despite many similarities to Karl in its mid-ocean origin and track through the Caribbean, Matthew developed rapidly, but failed to become a hurricane whereas Karl developed slowly and eventually formed into a major hurricane.

vii. Nicole

In the wake of Matthew a large gyre formed over Central America in which strong flow from the Eastern Pacific extended across Panama and Costa Rica into the Caribbean. The NHC initiated a tropical depression advisory to the east of Belize on the eastern side of this gyre at 15 UTC 28 September. The tropical depression tracked northeastward and became a weak tropical storm (Nicole) at 1500 UTC 29 September over central Cuba. Tropical storm Nicole tracked north-northeastward and dissipated subsequent to 2100 UTC 29 September in the Florida Strait.

The pre-genesis environment of Nicole was interesting because the storm appeared to originate out of a broad area of multiple low-level vorticity maxima that stretched from the Gulf of Tehuantepec to the Bay of Campeche and then eastward

across northern Guatemala and Belize to the southwestern Caribbean Sea. The presence of multiple low-level vorticity maxima on the east side of the larger gyre created great uncertainty in properly locating pouch PGI50. Model (GFS, ECMWF, UKMET, NOGAPS) uncertainty on the forecast track, duration, and intensity of Nicole was perhaps the largest of any TC during PREDICT. The Nicole case is of scientific interest for several reasons. First, what role did Mathew's pouch play in establishing this gyre complex? Second, did other disturbances from the east enter this region and influence the development of Nicole? Third, how does a developing system emerge from within a larger gyre complex possessing multiple low-level vorticity centers, with or without the support of a parent wave in the lower troposphere above the boundary layer? Fourth, this case provides an excellent testbed to TC genesis predictability experiments. Noteworthy is that the ECMWF ensemble anticipated the development of a major circulation center in this region ten days in advance.

viii. PGI48 (pre-Otto?)

The final mission of PREDICT was flown on September 30, the final day of the project. The target was a weak circulation centered near 13°N, 57°W associated with relatively disorganized convection across an area of nearly 1000 km. The circulation drifted northwestward over the following several days, and may have become entwined in the development of Hurricane Otto, a tropical transition event (Davis and Bosart 2004), on 5 October.

5. Lessons Learned and the Road Ahead

While we anticipate many research findings will arise from the careful analysis of PREDICT observations (in conjunction with observations taken during GRIP and IFEX), there were some clear lessons learned that are summarized here. First, the GV's ability to fly quickly to the target region at high altitude and safely navigate over or around deep convection proved that this sampling method, incorporated in the PREDICT proposal strategy, is highly effective for investigating tropical cyclogenesis in remote oceanic areas.

Another lesson learned is that tropical cyclogenesis may be more predictable than previously thought. PREDICT demonstrated that genesis regions could be targeted more than 2 days in advance, and in some cases four-day projections were useful. This is not to say that genesis itself was predictable on longer time scales, but our ability to anticipate the existence and approximate location of a pouch (and associated sweet spot) exceeded prior expectations of many of the PIs. Recall that the sweet spot is the intersection of the wave trough axis and the wave critical line. This translates to an enhanced ability to anticipate the path along which genesis may occur, even though the exact timing of genesis remains uncertain due to the chaotic influence resulting from moist convection.

A practical outcome is the realization of a trackable feature in forecast models that can be treated much the same way as a tropical cyclone center, long before an identifiable organized storm exists! The predictability of the track of the sweet spot manifests qualitatively similar predictability as the track of a tropical cyclone. In particular, this suggests that ensembles of global and regional models should be

effective in estimating a most likely path along which genesis can occur as well as providing the uncertainty in this path. While further research is necessary to quantify the predictability of "pouch tracks", we believe that the implications for improving tropical cyclone forecasts out to a week (the current goal of the National Hurricane Center), or perhaps even longer, using pouch tracking, are significant.

It became apparent also during PREDICT that the observations collected by the GV enhanced the subsequent skill of predicting the pouch track and pouch structure in operational and research models, and in several instances, the data enhanced the skill of the genesis prediction itself. This was most evident in ex-Gaston, Karl and Matthew during which several missions were flown. An important question is what aspect of the measurements was most important for enhancing predictive skill. Another practical question is how many flights are necessary to get cycling data assimilation systems on the right trajectory in model phase space. Research will seek also to understand the relative contributions of convective-scale (Sippel and Zhang 2008, 2010; Nguyen et al. 2008; Shin and Smith 2008; Zhang and Sippel 2009) and meso-synoptic-scale uncertainties toward the limits of predictability of genesis.

A potentially significant link between the dynamics and thermodynamics of the non-developing Gaston case was suggested by the shallowing of Gaston's pouch over the five-day observation period. A deteriorating pouch is hypothesized to enable the intrusion of middle-level dry air from outside with correspondingly low θ_e values. Such a link between dynamics and thermodynamics points to the usefulness of obtaining in situ data for characterizing the thermodynamic and kinematic structure of candidate wave-

pouches. Further research is required for this case as well as the other developing and non-developing cases observed during PREDICT.

Acknowledgements

References

Anthes, R. A., et al., 2008: The COSMIC/FORMOSAT-3 Mission: Early results. *Bull. Amer. Meteor. Soc.*, **89**, 313–333.

Bister, M., and K. A. Emanuel, 1997: The genesis of Hurricane Guillermo: TEXMEX analyses and a modeling study. *Mon. Wea. Rev.*, **125**, 2662—2682.

Davis, C. A. and L. F. Bosart, 2004: The TT problem: forecasting the tropical transition of cyclones. *Bull. Amer. Meteorol. Soc.*, **85**, 1657–1662.

DeMaria, M., J.A. Knaff, and B.H. Connell, 2001: A Tropical Cyclone Genesis Parameter for the Tropical Atlantic*. Wea. Forecasting*, **16**, 219–233.

Dunion, J.P., and C.S. Velden, 2004: The Impact of the Saharan Air Layer on Atlantic Tropical Cyclone Activity. *Bull. Amer. Meteor. Soc.*, **85**, 353–365.

Dunion, J. P., and C. S. Marron, 2008: A reexamination of the Jordan mean tropical sounding based on awareness of the Saharan Air Layer: Results from 2002. *J. Climate*, **21**, 5242- 5253.

Dunion, J.P., 2011: Re-Writing the Climatology of the Tropical North Atlantic and Caribbean Sea Atmosphere. J. Climate. 24 no. 3, 893-908.

Dunkerton, T. J., Montgomery, M. T., and Wang, Z., 2009: Tropical cyclogenesis in a tropical wave critical layer: easterly waves. *Atmos. Chem. & Phys.*, **9**, 5587-5646.

Dvorak, V., 1975: Tropical cyclone intensity analysis and forecasting from satellite imagery. *Mon. Wea. Rev.*, **103**, 420-430.

Elsberry, R. L., and P. A. Harr (2008), Tropical cyclone structure (TCS08) field experiment science basis, observational platforms, and strategy. *Asia Pac. J. Atmos. Sci.,* **44**, 209–231.

Emanuel K. A. 1994: **Atmospheric convection**. Oxford University Press: Oxford, UK.

Emanuel, K. A., 2005: **Divine Wind: The history and science of hurricanes**. Oxford University Press, New York, 285 pp.

Evan, A., J. Dunion, J. Foley, A. Heidinger, and C. Velden, 2006: New evidence for a relationship between Atlantic tropical cyclone activity and African dust outbreaks. *Geophys. Res. Lett.*, **33**, L19813, doi:10.1029/2006GL026408.

Fang, J and F. Zhang, 2010: Initial development and genesis of Hurricane Dolly (2008). *J. Atmos. Sci*, **67**, 655-672.

Fang, J and F. Zhang, 2011: Evolution of Multi-scale Vortices in the Development of Hurricane Dolly (2008). *J. Atmos. Sci.*, **68**, 103-122.

Frank, N. L., 1970: Atlantic tropical systems of 1969. *Mon. Wea. Rev.,* **98**, 307–314.

Garrison, J. L., M. Walker, J. S. Haase, T. Lulich, F. Xie, B. D. Ventre, M. H. Boehme, B. Wilmhoff, and S. J. Katzberg, 2007: Development and Testing of the GISMOS Instrument. Paper presented at IEEE International Geoscience and Remote Sensing Symposium. Barcelona, Spain, 23-27 July 2007.

Gray, W. M.,1968: Global view of the origin of tropical disturbances and storms, Mon. Wea. Rev., **96**, 669– 700.

Gray, W. M., 1998: The formation of tropical cyclones. *Meteorol. Atmos. Phys.*, **67**, 37-69.

Halverson, J., Black, M., Braun, S., et al.: NASA's Tropical Cloud Systems and

    Processes Experiment, *Bull. Amer. Meteor. Soc.*, **88**, 867–882, 2007.

Hawkins, J., and C. Velden, 2011: Supporting Meteorological Field Experiment Missions

    and Post-Mission Analysis with Satellite Digital Data and Products. Accepted in

    BAMS.

Herman, R. L. and A. J. Heymsfield, 2003: Aircraft icing at low temperatures in Tropical

    Storm Chantal. Geophys. Res. Lett., 30, 1955, doi:10.1029/2003GL017746.

James, R. P. and P. M. Markowski, 2009: A numerical investigation of the effects of dry

    air aloft on deep convection. *Mon. Wea. Rev.*, **137**, 140-161.

Jones, T. A., D. J. Cecil, and J. Dunion, 2007: The environmental and inner-core condi-

    tions governing the intensity of Hurricane Erin (2007). *Wea. Forecasting*, **22**, 708-

    725.

McBride, John L., Raymond Zehr, 1981: Observational Analysis of Tropical Cyclone

    Formation. Part II: Comparison of Non-Developing versus Developing Systems.

    J. Atmos. Sci., **38**, 1132-1151.

McWilliams, J., 1984: The emergence of isolated coherent vortices in turbulent flow. *J.

    Fluid Mech.*, **146**, 21–43.

Meng, Z, and F. Zhang, 2008a: Test of an ensemble-Kalman filter for mesoscale and

    regional-scale data assimilation. Part III: Comparison with 3Dvar in a real-data

    case study. *Mon. Wea. Rev.*, **136**, 522-540.

Meng, Z, and F. Zhang, 2008b: Test of an ensemble-Kalman filter for mesoscale and regional-scale data assimilation. Part IV: Performance over a warm-season month of June 2003. *Mon. Wea. Rev.*, **136**, 3671-3682.

Montgomery, M. T., Lussier III, L. L., Moore, R. W., and Wang, Z., 2010a: The genesis of Typhoon Nuri as observed during the Tropical Cyclone Structure 2008 (TCS-08) field experiment – Part 1: The role of the easterly wave critical layer. *Atmos. Chem. & Physics,* **10**, *9879-9900*.

Montgomery, M. T., Z. Wang, and T. J. Dunkerton, 2010b: Coarse, intermediate and high resolution numerical simulations of the transition of a tropical wave critical layer to a tropical storm. *Atmos. Chem. & Physics*, **10,** *10803-10827.*

Montgomery, M. T. and R. K. Smith, 2010: Tropical-Cyclone Formation: Theory and Idealized modeling. Topic 2.1 of Seventh International Workshop in Tropical Cyclones, 23 pp.; Workshop held in November 2010 in La ReUnion. J. Kepert and J. Chan. Editors.

Montgomery M. T., M. E. Nicholls, T. A. Cram and A. B. Saunders, 2006: A vortical hot tower route to tropical cyclogenesis. *J. Atmos. Sci*., **63,** 355-386.

Nguyen, V. S., R. K. Smith, M. T. Montgomery, 2008: Tropical-cyclone intensification and predictability in three dimensions, *Q. J. R. Meteorol. Soc., **134,** 563-582.*

Raymond, D. J., C. L'opez-Carillo, and L. L'opez-Cavazos, 1998: Case-studies of developing east Pacific easterly waves. *Quart. J. Roy. Meteor. Soc.*, **124**, 2005—2034.

Raymond, D. J. and López Carrillo, C., 2011: The vorticity budget of developing Typhoon Nuri (2008). *Atmos. Chem. & Physics*, **11**, 147–163.

Reale, O., W. K. Lau, K.-M. Kim, and E. Brin, 2009: Atlantic tropical cyclogenetic processes during SOP-3 NAMMA in the GEOS-5 global data assimilation and forecast system. *J. Atmos. Sci.*, **66**, 3563-3578.

Reasor, P. D., M. T. Montgomery and L. F. Bosart. 2005: Mesoscale observations of the genesis of Hurricane Dolly (1996). *J. Atmos. Sci.*, **62**, 3151–3171.

Sadler, J.C., 1976: A role of the tropical upper troposphere in typhoon development. *Mon. Wea. Rev.*, **104**, 1266-1278.

Shin S Smith RK. 2008 Tropical-cyclone intensification and predictability in a minimal three-dimensional model. *Quart. J. Roy. Meteor. Soc.*, **134**, 1661-1671.

Shu, S., and L. Wu, 2009: Analysis of the influence of the Saharan air layer on tropical cyclone intensity using AIRS/Aqua data. *Geophys. Res. Lett.,* **36**, doi:10.1029/2009GL037634.

Sippel, J. A., and F. Zhang, 2008: Probabilistic evaluation of the dynamics and predictability of tropical cyclogenesis. *J. Atmos. Sci,,* **65***,* 3440–3459.

Sippel, J. A and F. Zhang, 2010: Factors affecting the predictability of hurricane Humberto (2007). *J. Atmos. Sci,,* **67**, 1759-1778.

Skamarock, W. C., Klemp, J. B., Dudhia, J., Gill, D. O., Barker, D. M., Wang, W., and Powers, J. G., 2005: A description of the Advanced Research WRF Version 2. NCAR Tech. Note/TN-468+STR, 88 pp.

Sun, D., W. K. M. Lau, M. Kafatos, Z. Boybeyi, G. Leptoukh, C. Yang, and R. Yang, 2009:Numerical simulations of the impacts of the Saharan Air Layer on Atlantic tropical cyclone development. *J. Climate*, **22**, 6230-6250.

Torn, R. D., and G. J. Hakim, 2008: Ensemble-based Sensitivity Analysis. *Mon. Wea. Rev.*, **136**, 663–677.

Torn, R. D., 2010: Performance of a Mesoscale Ensemble Kalman Filter (EnKF) During the NOAA High-Resolution Hurricane Test. *Mon. Wea. Rev.*, **138**, 4375-4392.

Wang, Z., M. T. Montgomery, and T. J. Dunkerton, 2010a: Genesis of Pre hurricane Felix (2007). Part I: The Role of the Wave Critical Layer. *J. Atmos. Sci.*, **67**, 1711-1729.

Wang, Z., M. T. Montgomery, and T. J. Dunkerton, 2010b: Genesis of Pre-hurricane Felix (2007). Part II: Warm core formation, precipitation evolution and predictability. *J. Atmos. Sci.*, **67**, 1730-1744.

Wang, Z., M. T. Montgomery, and T. J. Dunkerton, 2009: A dynamically-based method for forecasting tropical cyclogenesis location in the Atlantic sector using global model products. *Geophys. Res. Lett.*, **36**, L03801, doi:10.1029/2008GL035586.

Wang, Z., M. T. Montgomery, and C. Fritz, 2010: A first look at the structure of the wave pouch during the 2009 PREDICT-GRIP "dry run" over the Atlantic, *Mon. Wea. Rev., accepted.*

Weiss, J., 1991: The dynamics of enstrophy transfer in two-dimensional hydrodynamics. *Physica D: Nonlinear Phenomena* **48**, Issues 2-3, pgs. 273-294.

Wimmers, A. J. and C. S. Velden, 2007: MIMIC: A new approach to visualizing satellite microwave imagery of tropical cyclones. *Bull. Amer. Meteor. Soc.*, **88**, 1187-1196.

Wimmers, A.J. and C.S. Velden, 2011: Seamless Advective Blending of Total Precipitable Water Retrievals from Polar Orbiting Satellites. Accepted in *J. Appl. Meteor. Climate.*

Wu, L., 2007: Impact of Saharan air layer on hurricane peak intensity. *Geophys. Res. Lett.,* **34**,10 doi:10.1029/2007GL029564.

Xie, F., J. S. Haase, and S. Syndergaard (2008), Profiling the Atmosphere Using the Airborne GPS Radio Occultation Technique: A Sensitivity Study, *Trans. IEEE Geosci. and Remote Sens.*, **46**(11), 3424-3435.

Zhang, F. and J. A. Sippel, 2009: Effects of moist convection on hurricane predictability. *J. Atmos. Sci,*, **66**, 1944-1961.

Zhang, F., Y. Weng, J. A. Sippel, Z. Meng, and C. H. Bishop, 2009: Cloud-resolving Hurricane Initialization and Prediction through Assimilation of Doppler Radar Observations with an Ensemble Kalman Filter: Humberto (2007). *Mon. Wea. Rev,* **137**, 2105-2125.

Zipser, E.J., C.H. Twohy, S.C. Tsay, K.L. Thornhill, S. Tanelli, R. Ross, T.N. Krishnamurti, Q. Ji, G. Jenkins, S. Ismail, N.C. Hsu, R. Hood, G.M. Heymsfield, A. Heymsfield, J. Halverson, H.M. Goodman, R. Ferrare, J.P. Dunion, M. Douglas, R. Cifelli, G. Chen, E.V. Browell, and B. Anderson, 2009: The Saharan Air Layer

and the Fate of African Easterly Waves—NASA's AMMA Field Study of Tropical Cyclogenesis. *Bull. Amer. Meteor. Soc.*, **90**, 1137–1156.

Table 1. Instrumentation payload on the NSF/NCAR GV research aircraft.

State parameters	Pressure	
	Temperature (3x)	
	Dewpoint	Buck Research
	Water vapor density	VCSEL and CARI TDL
Position	Honeywell IRS	
	Novatel GPS	
3-D wind	Dynamic pressure (2x)	Honeywell
	Attack/sideslip	Honeywell in radome
	Attack/sideslip	Honeywell in gust pod
Microphysics	Icing rate	Rosemount
	Liquid water content	DMT King probe
	Cloud droplets/ice	DMT CDP probe
	Ice particles	PMS/DMT 2D-C
	Ice particles	SPEC 3V-CPI
	Condensation nuclei	TSI water CN
	Aerosol particles	DMT UHSAS
	Aerosol particles	CVI
Remote sensing	Temperature profile	JPL Microwave Temperature Profiler
	Water vapor profile	Purdue GISMOS
	True air speed	EOL LAMS
Dropsondes	Pressure, temperature, dewpoint, wind	EOL/Vaisala GPS sondes

SYSTEM	Description	First Identification	First Mission	First NHC Advisory	Flights (Days)	Drops
PGI27	Non-developing African wave	08 August	August 17	None	2 (2)	48
PGI30	Non-developing African wave	14 August	August 21	None	2 (2)	38
PGI36 (Fiona)	Developed African wave	25 August	August 30	21 UTC 30 August	3 (3)	83
PGI38 (ex-Gaston)	Failed redevelopment of African wave	28 August	September 2	15 UTC 1 September	5 (5)	109
PGI44 (Karl)	Developing non-African wave	9 September	September 10	21 UTC 14 September	6 (5)	127
PGI46 (Matthew)	Developing non-African wave	16 September	September 20	18 UTC 23 September	4 (4)	83
PGI50 (Nicole)	Developing Caribbean gyre	26 September	September 28	15 UTC 28 September	2 (2)	47
PGI48	May have become Otto	26 September	September 30		1 (1)	26

Table 2. Disturbances investigated with the GV, along with origin of pre-depression disturbance, date "pouch tracking" began, date of first mission, date and time of genesis as declared by NHC (if it occurred), number of GV missions and days flown, and number of successful dropsondes.
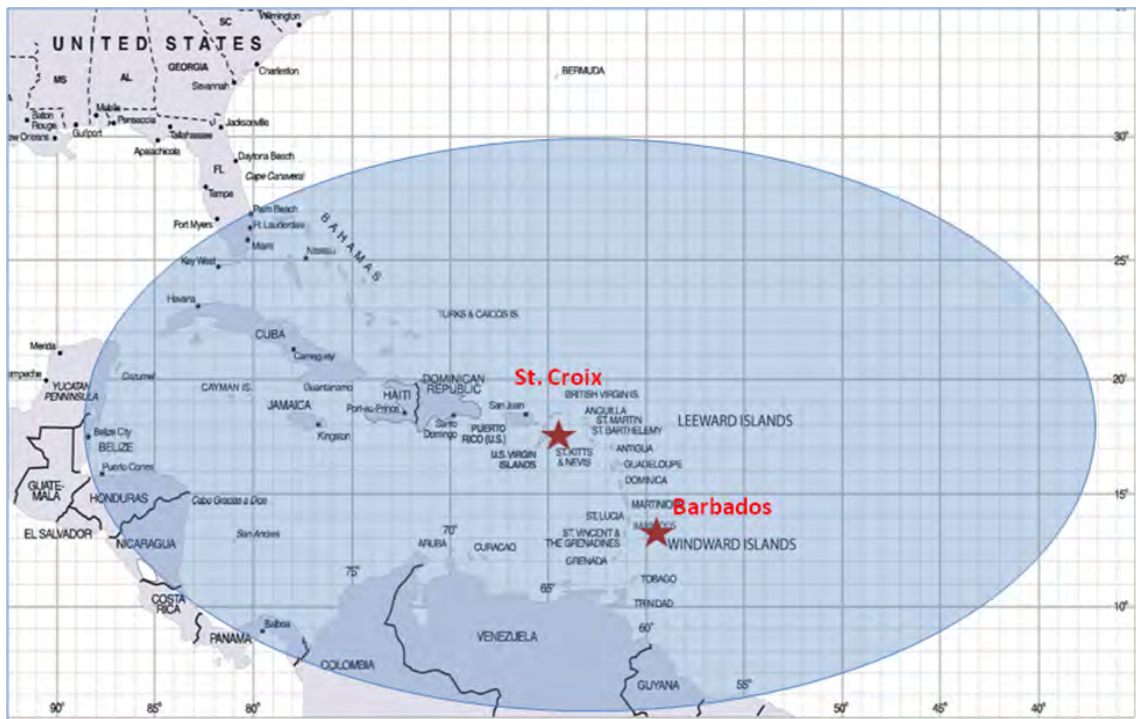
Figure 1. PREDICT domain. The primary base of operations was St. Croix, USVI, with an alternate of Barbados.
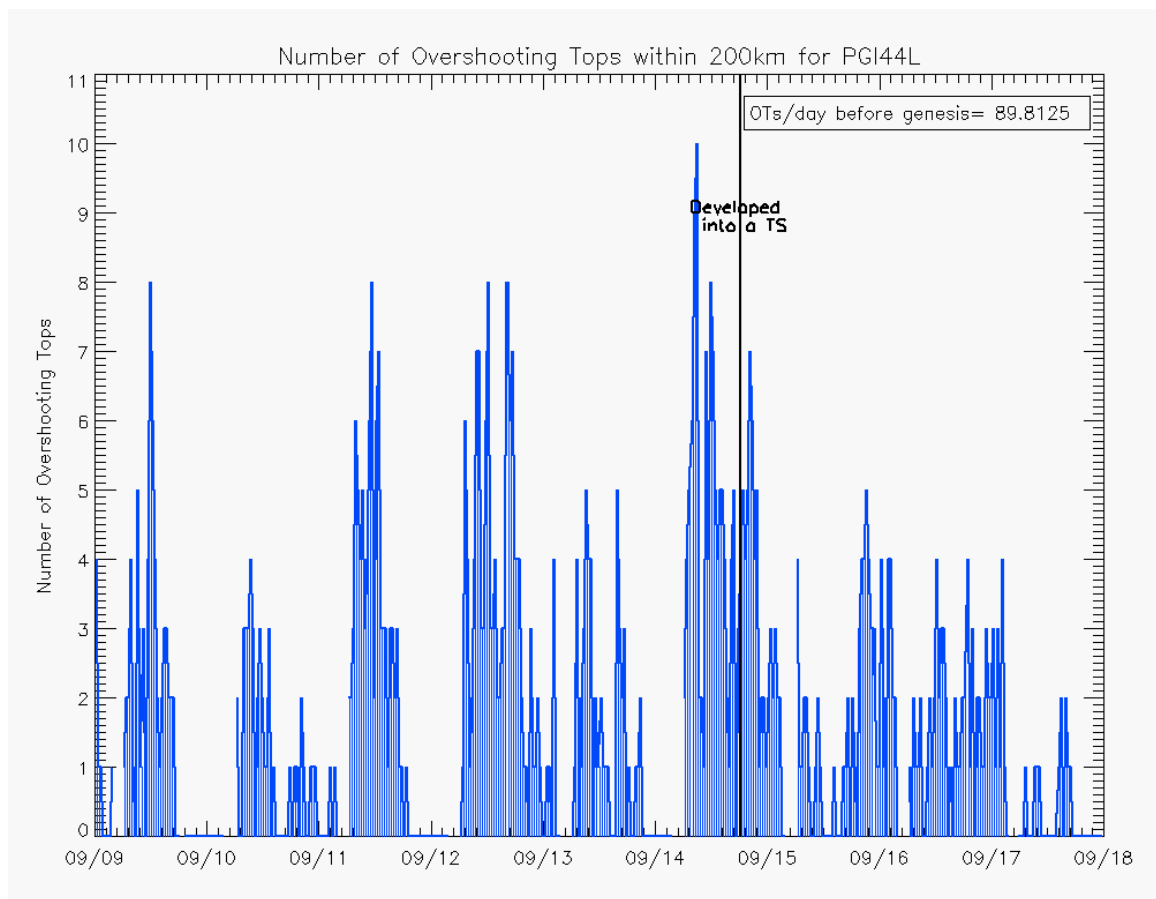
Figure 2. Time-series of overshooting tops derived from the CIMSS cloud-top product prior to and during the genesis of Karl (PGI44).
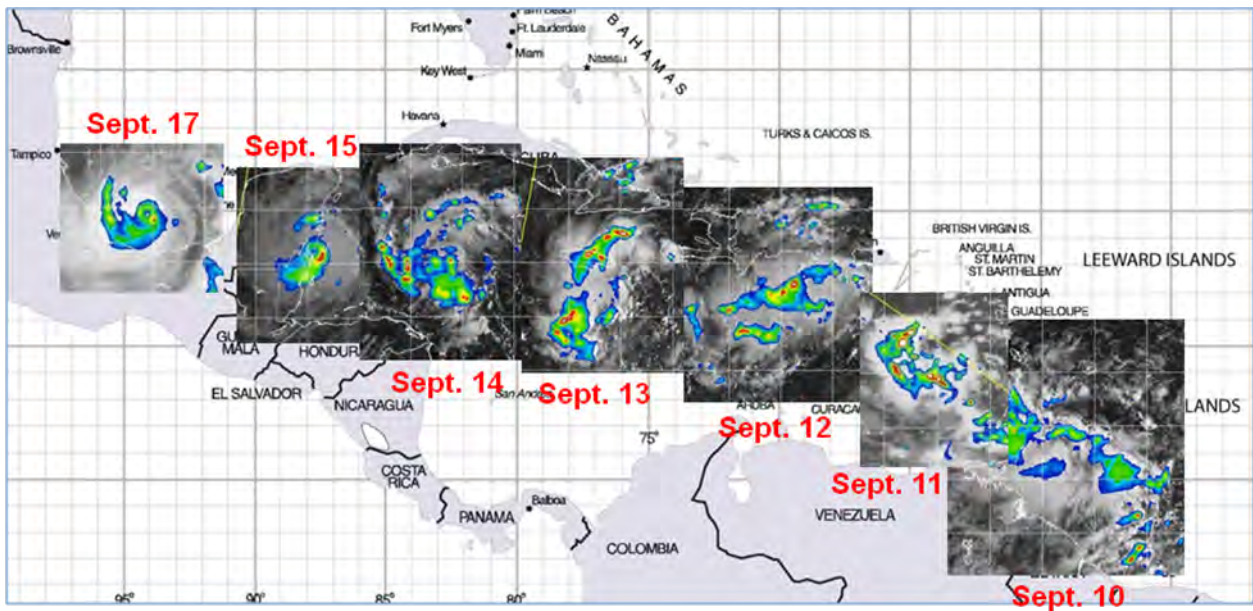
Figure 3. 85 GHz montage (images courtesy of NRL-Monterey) for the active convection periods on each day from Sept. 10-17 (excluding 16 Sept) during the genesis of Karl (PGI44). Note the small eye on the Yucatan coast on 15 September.
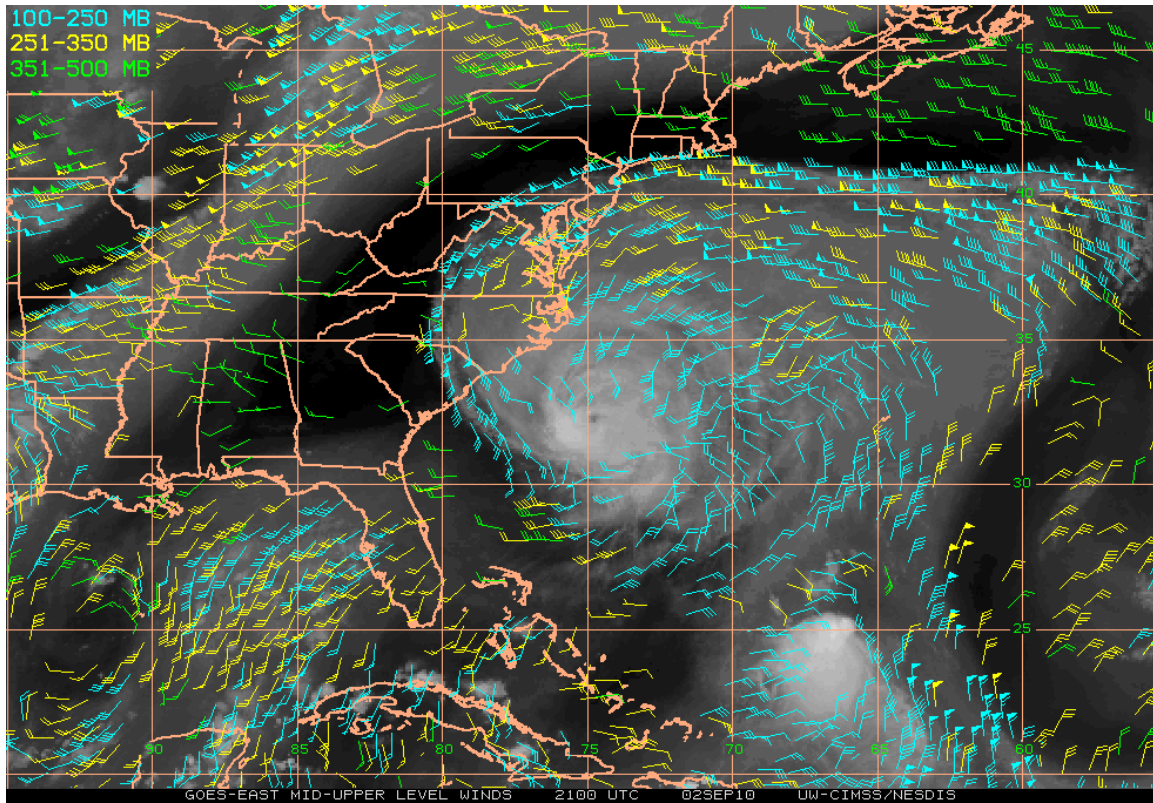
Figure 4. Plot of upper-level satellite winds at 21 UTC on 2 September 2010. The image is centered on Hurricane Earl, with its upper-level outflow producing an impinging vertical shear on tropical storm Fiona (formerly PGI36) that is located east of the Bahamas.
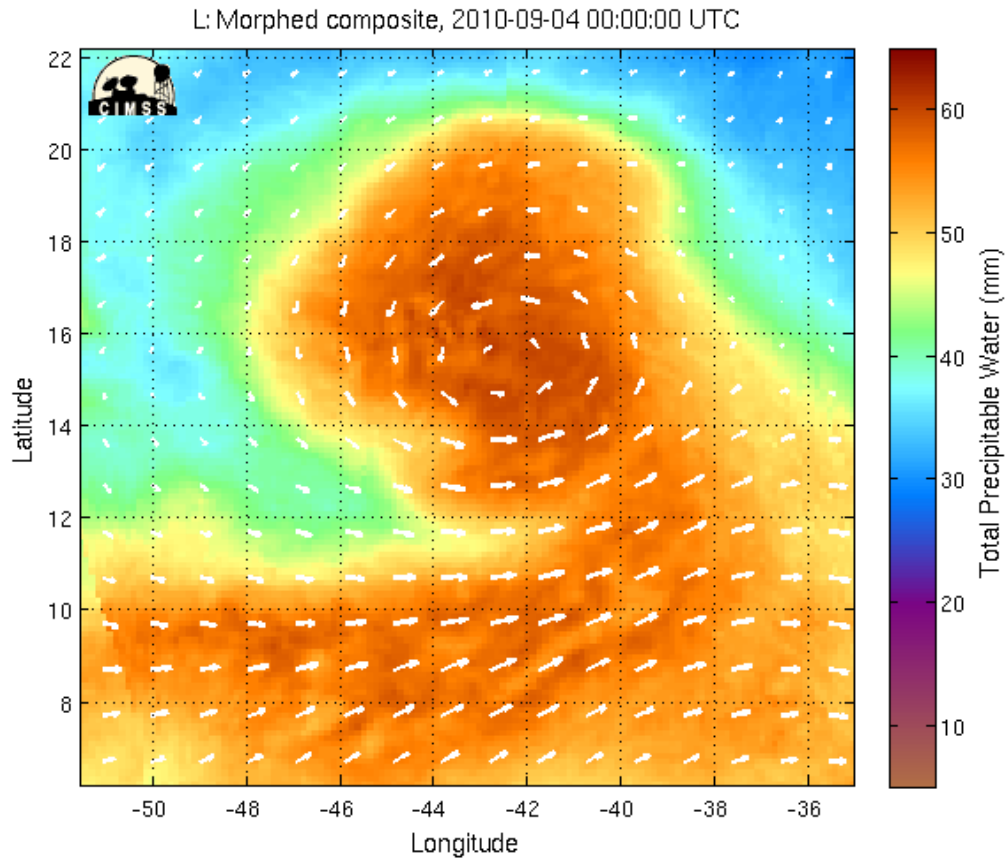
Figure 5. Mosaic of total precipitable water (TPW, units mm) and system-relative winds at 850 hPa valid 00 UTC 4 September, approximately 4 hours after the G-V concluded its second mission into PGI38 (ex-Gaston).
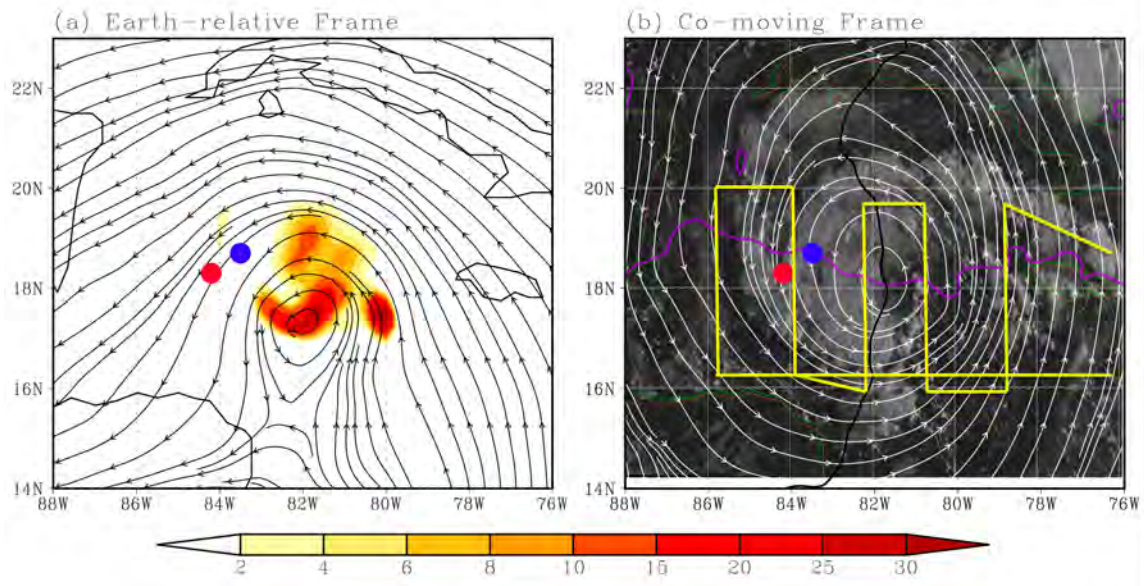
Figure 6.　Left: ECMWF 36-hour forecast of 700-hPa Earth-relative streamlines and OW (shading; units: $10^{-9}s^{-2}$) centered on wave-pouch PGI44/AL92 (pre-Karl) valid at 12 UTC 14 September 2010.　Right: Streamlines in the co-moving frame of reference (phase speed of 6.2 m/s westward), GOES visible imagery at 1225 UTC and flight pattern of G-V aircraft (yellow track). In the right figure, the black curve represents the trough axis, and the purple curve the local critical latitude defined by U = c_x. The red dot represents the actual genesis location, and the blue dot is the ECMWF 700-hPa predicted sweet spot, defined by the intersection of the trough axis (black curve) and critical latitude (purple curve), at 21 UTC 14 September 2010.
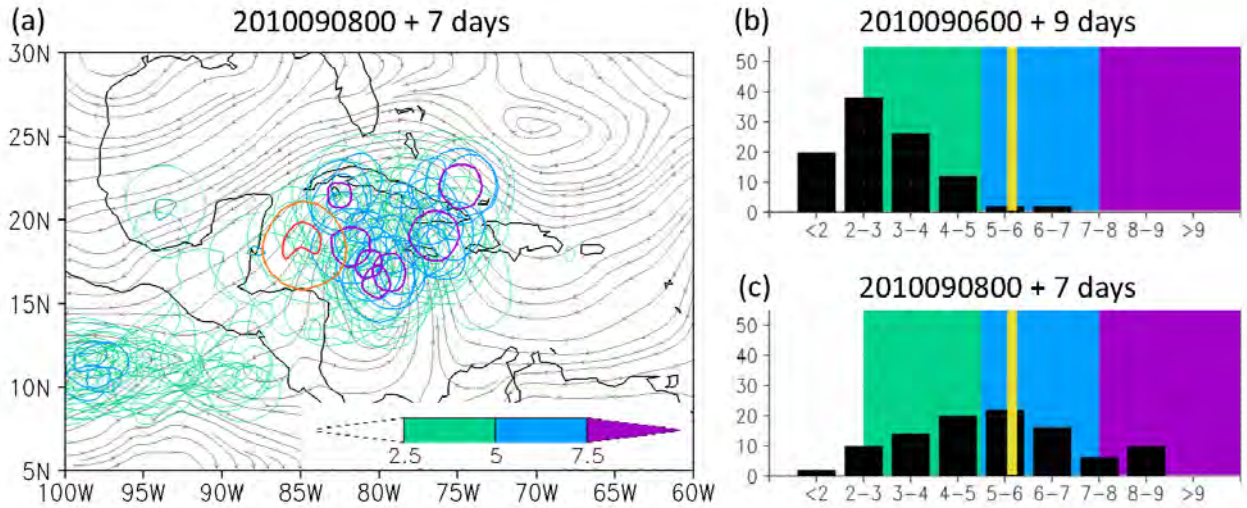
Figure 7. (a) 7-day, 50-member ECMWF ensemble predictions for PGI44 (pre-Karl), initialized at 0000 UTC 8 September 2010, of relative vorticity averaged over the 700-850 hPa layer and an area of radius 300 km. Contours of 2.5, 5 and 7.5 x 10^{-5} s^{-1} are illustrated. The corresponding ECMWF analysis at 0000 UTC 15 September 2010 is given by the orange (2.5 x 10^{-5} s^{-1}) and red (5 x 10^{-5} s^{-1}) contours. Right panels: Probability Distribution Function of maximum averaged relative vorticity within a box of 12-24N 90-70W for (b) 9-day ECMWF ensemble forecast initialized at 0000 UTC 6 September 2010 and (c) 7-day ECMWF ensemble forecast initialized at 0000 UTC 8 September 2010. The shaded colors correspond to the contour values in (a), and the verifying value of 5.65 x 10^{-5} s^{-1} in the ECMWF analysis at 0000 UTC 15 September 2010 is given by the vertical yellow line.
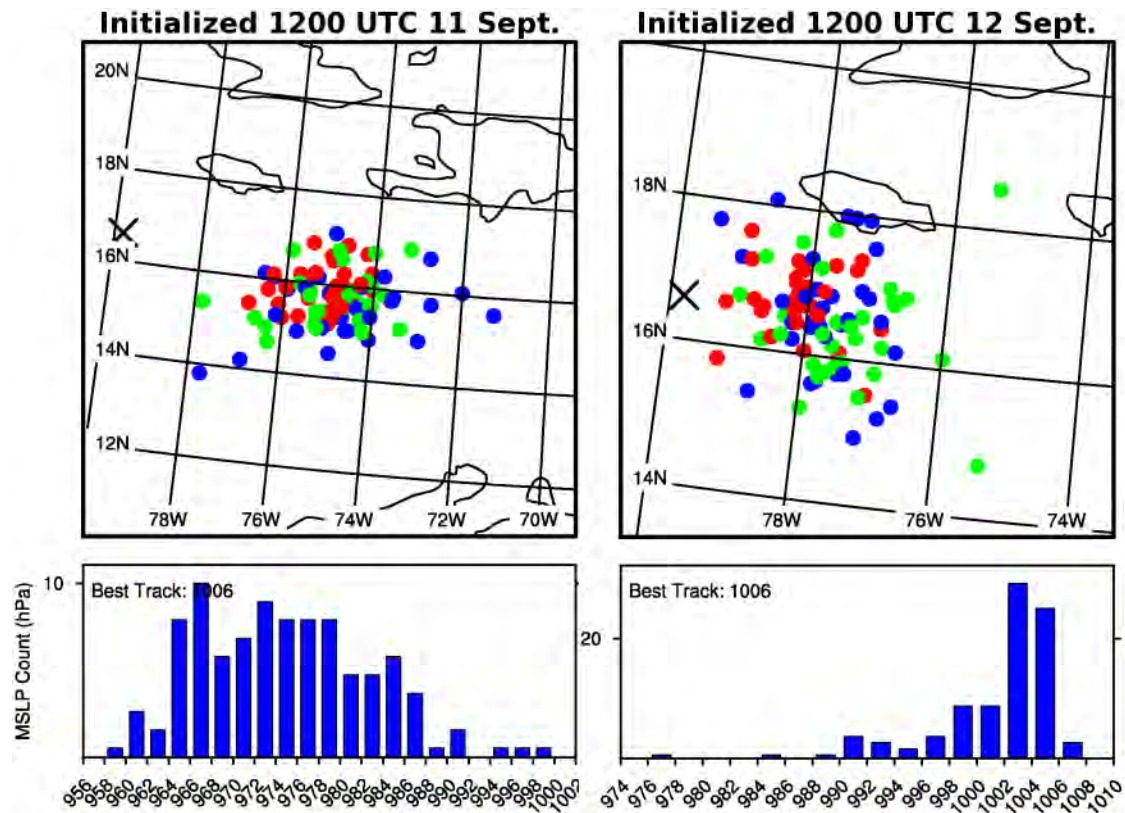
Figure 8: Ensemble forecasts of PGI44's position (top row) and minimum sea-level pressure (bottom row) initialized 1200 UTC 11 September 2010 (left column) and 1200 UTC 12 September 2010 (right column) valid 0000 UTC 14 September. The red (blue) dots denote the 1/3 of members with the lowest (highest) minimum SLP, while the green dotes denote the middle 1/3 of members. The X denotes the verification position.
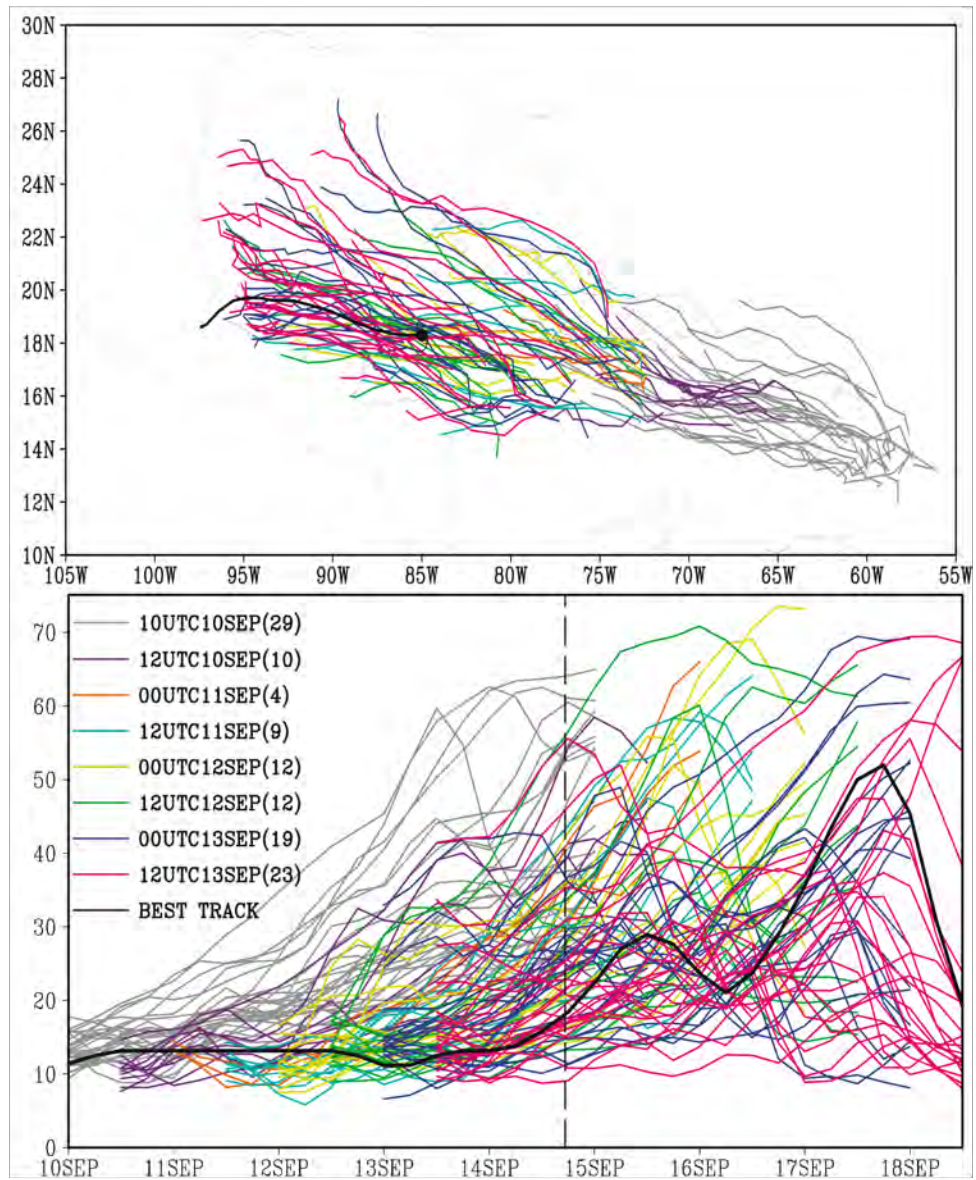
Figure 9: Track and intensity forecasts of PGI44 (pre-Karl) by 8 consecutive sets of 30-member 4.5-km 120-h WRF ensemble forecasts initialized from the PSU real-time hybrid EnKF analysis. Only ensemble members that reach the intensity of TC genesis are plotted with the number of members at different times shown in the bracket.
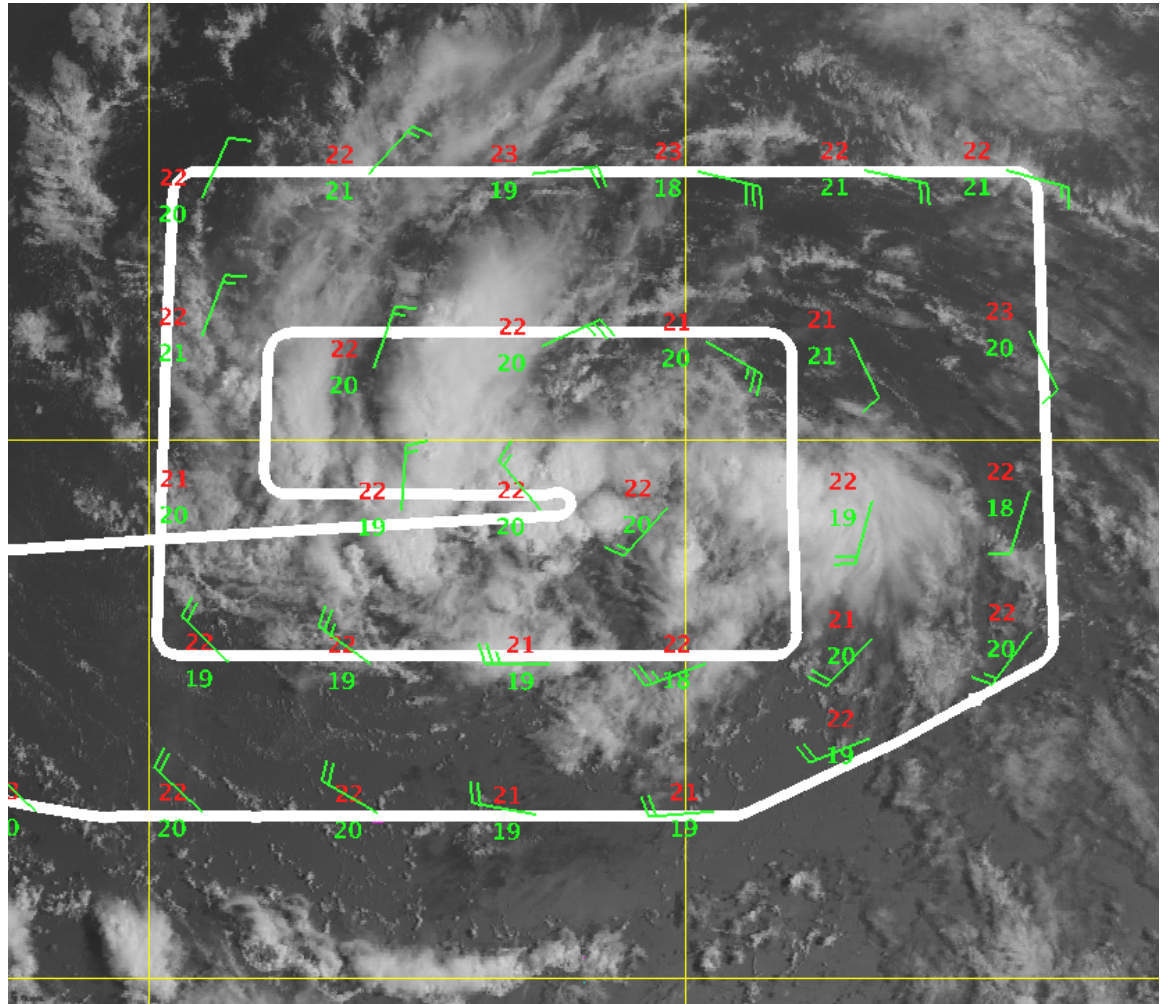
Figure 10. Dropsondes and flight track from the first G-V flight into PGI36 (soon after designated tropical storm Fiona by NHC) on August 30. Shown are wind, temperature (red) and dewpoint (green) at 900 hPa centered roughly on 13 UTC. The flight track is indicated by the thick-white line segments. GOES-visible satellite image is from 1315 UTC.
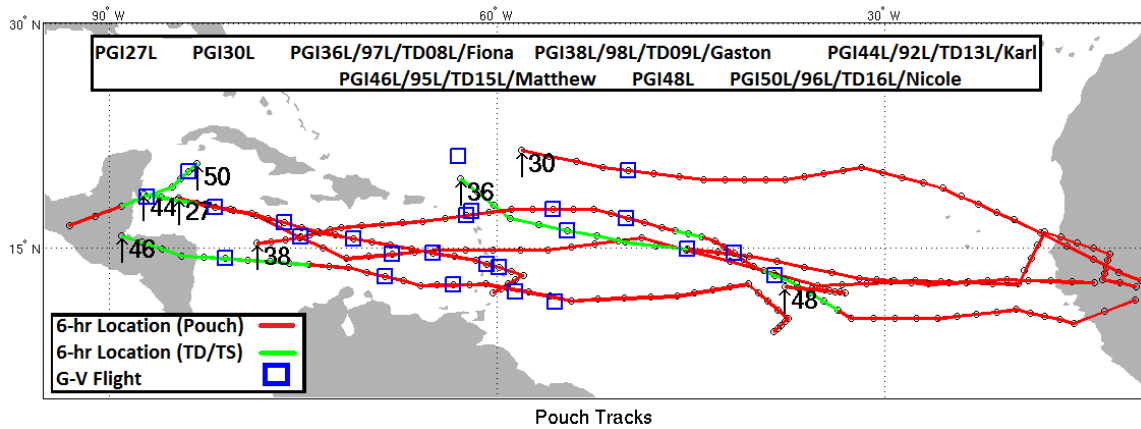
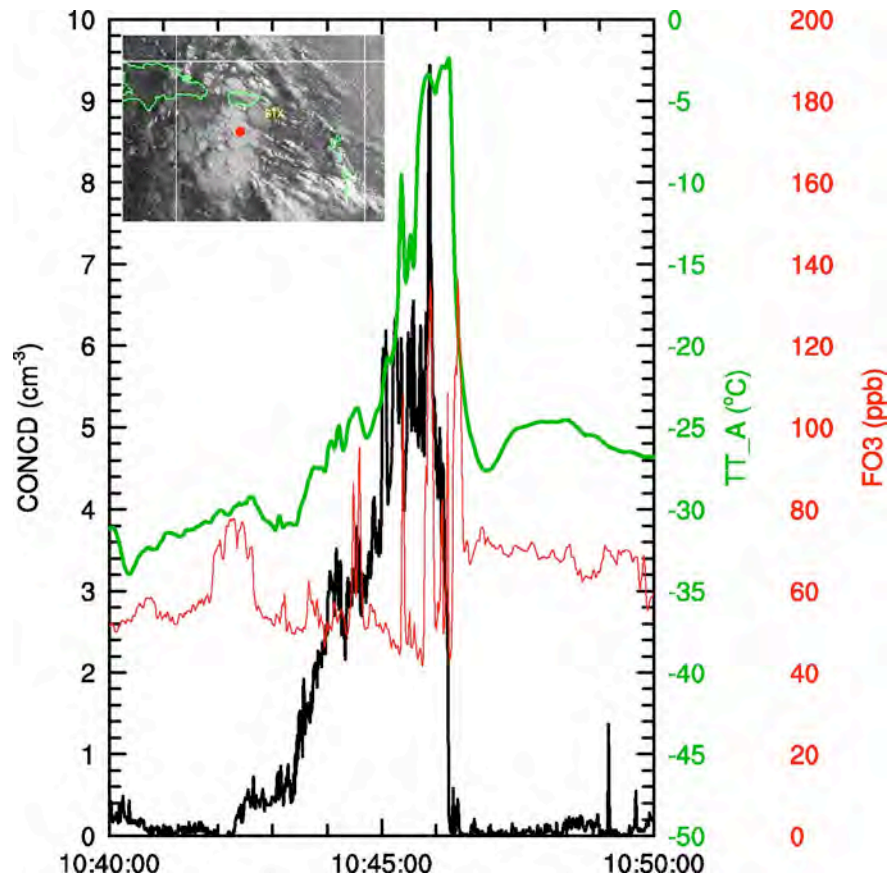Figure 11. Pouch tracks for systems that were flown by the G-V during PREDICT. The values at the track endpoints indicate the PGI number designations.

Figure 12. Time series of small ice particle concentration (CONCD, black curve), total air temperature (TT_A, green curve), and ozone mixing ratio (FO3, red curve) during the encounter with a high IWC region penetrated during RF02. The satellite image, valid at 1045 UTC, is shown at upper left with the location of the G-V indicated by the red dot at this time. Figure provided by J. Jensen and T. Campos, NCAR Earth Observing Laboratory.
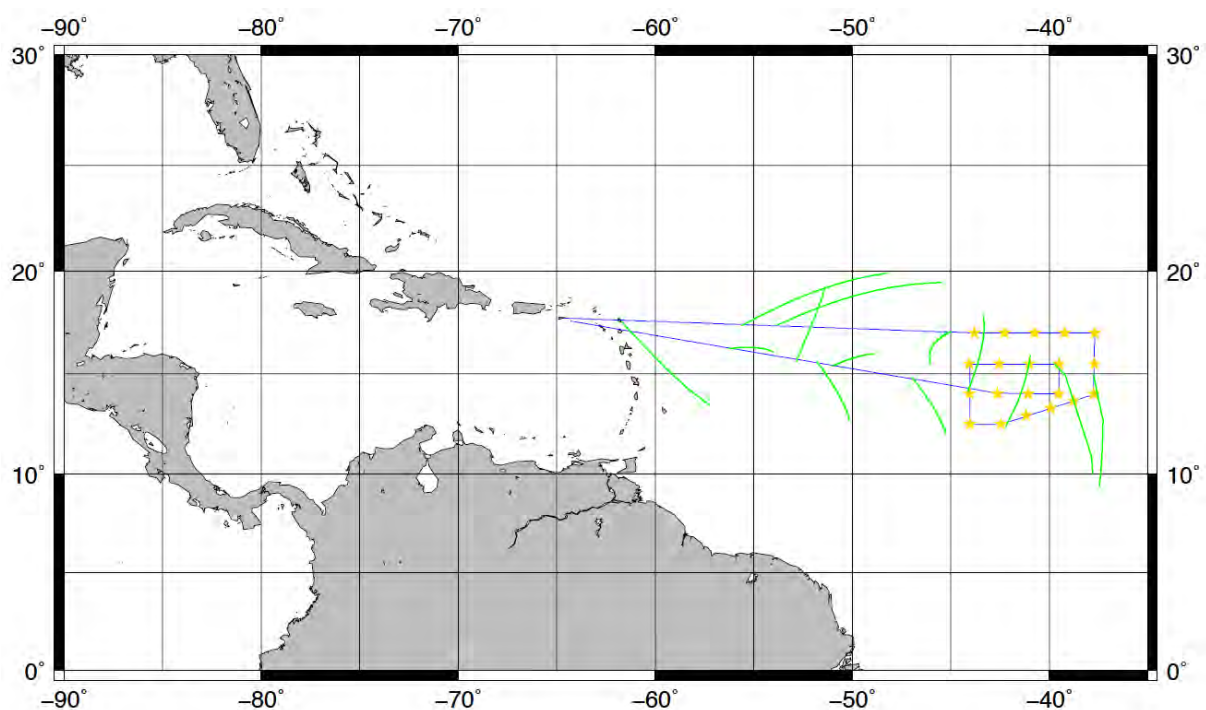
Figure 13. G-V flight track (blue), dropsonde locations (yellow) and sample horizontal projections of occultation paths on 2 September during the first mission into PGI38 (ex-Gaston).

Figure 14. Comparison of pouch-mean soundings of virtual potential temperature (θ_v) (red) and pseudo-equivalent potential temperature (θ_e) (blue) as a function of height derived from the G-V dropsondes in (a) the pouch of PGI38 (ex-Gaston) that failed to redevelop, and (b) the pouch of PGI44 (pre-Karl) that did develop. Numbers on curves refer to the day of the flight mission in September 2010.
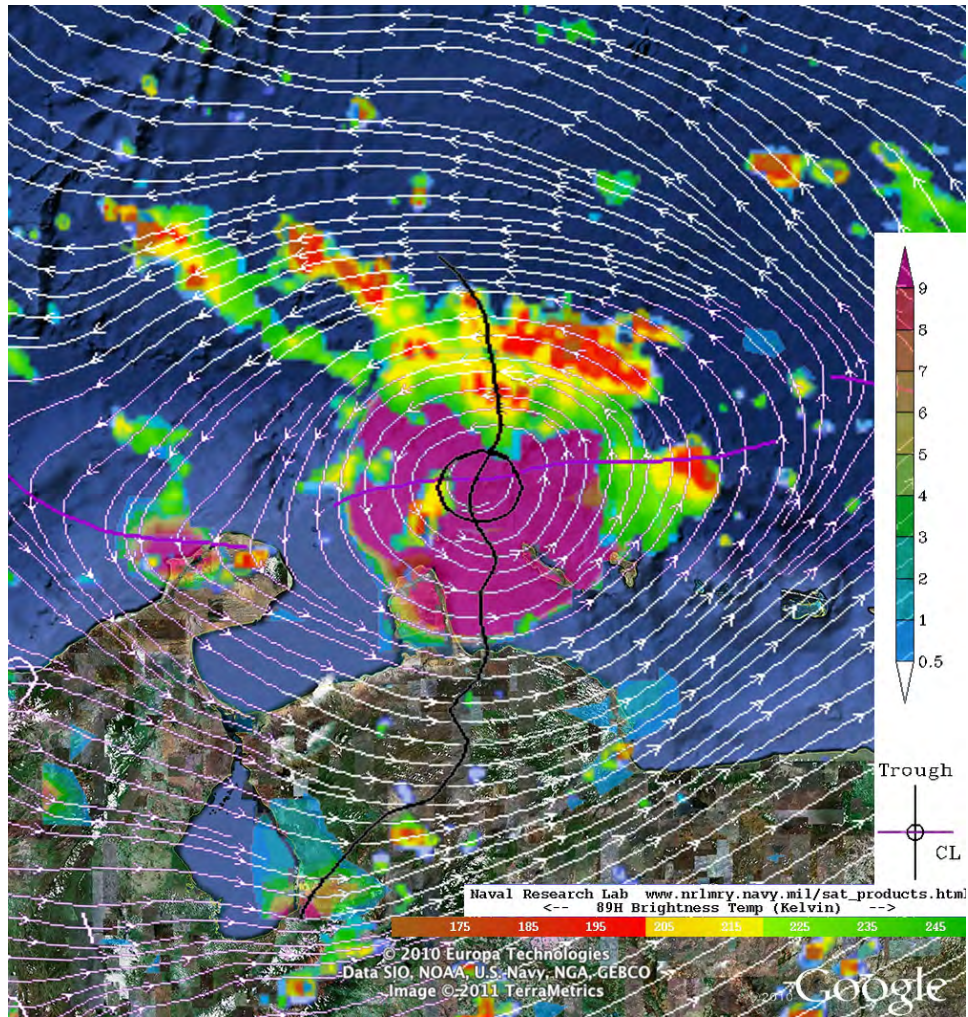
(a)

100910 − 100914   PGI44
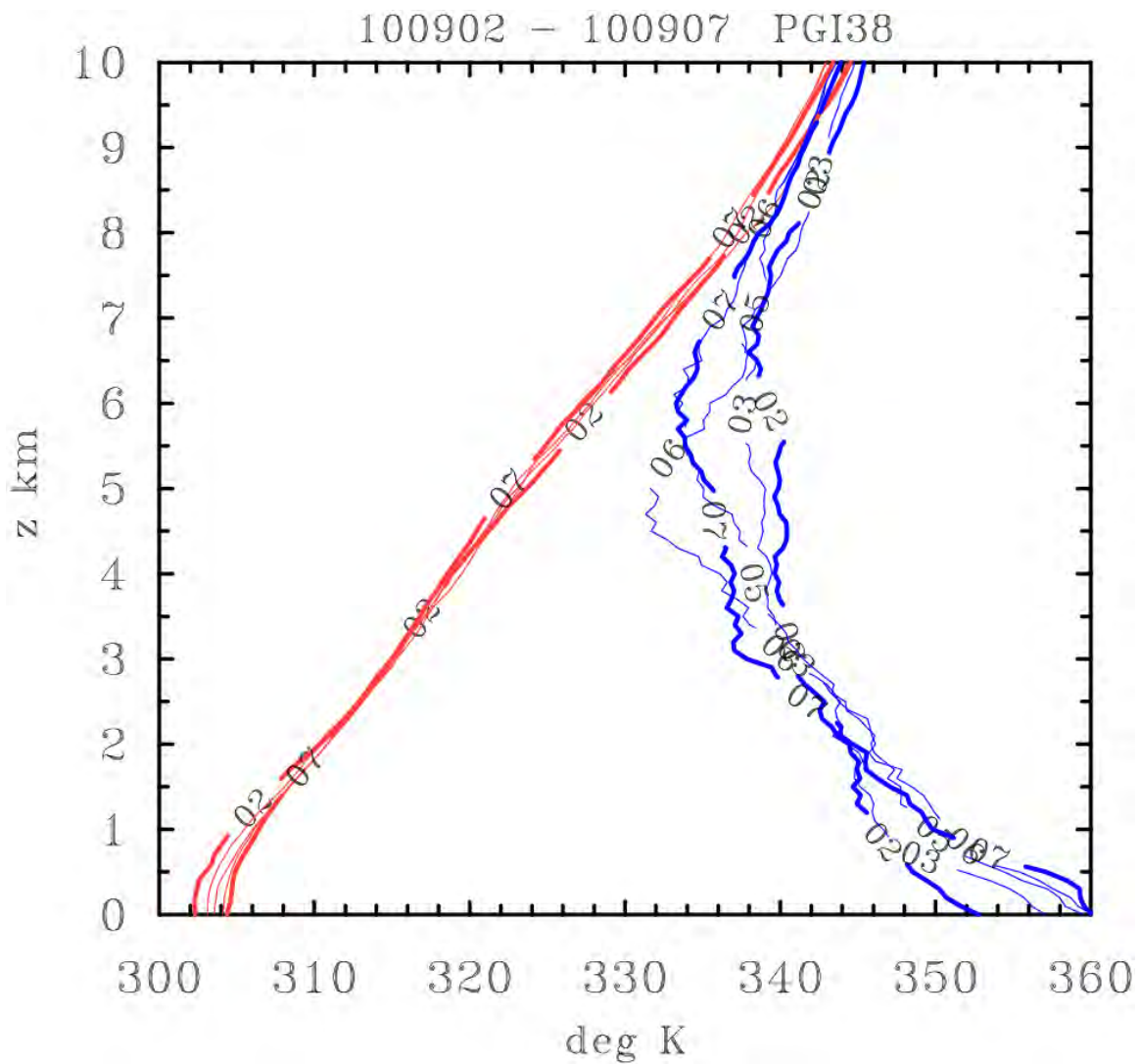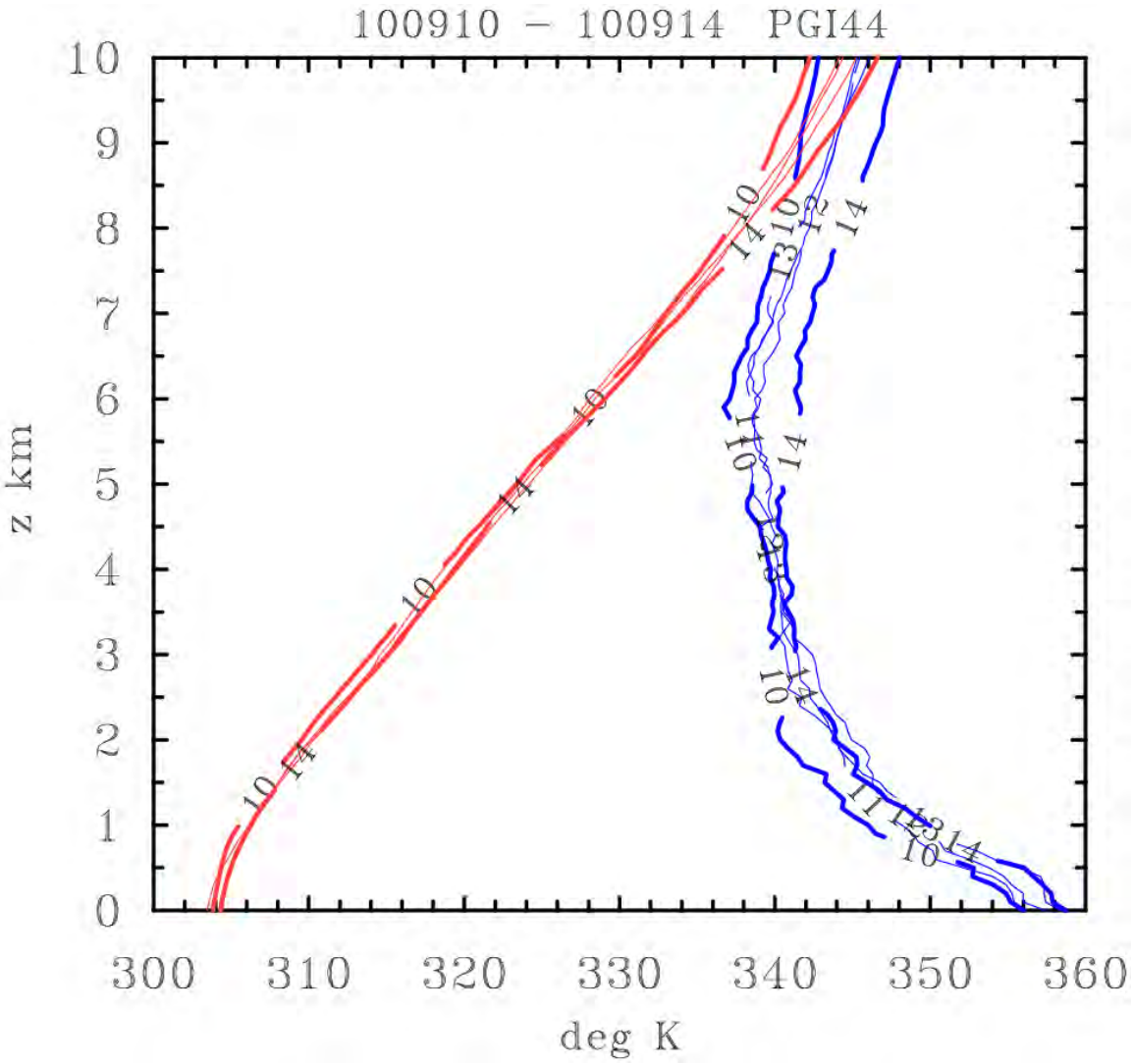
Figure 15. Co-moving streamlines (white) and regions of positive OW with cyclonic vorticity (light-blue and purple, color bar units of $10^{-9}s^{-2}$) at 700 hPa at 12 UTC 22 September derived from the ECMWF analysis. Superposed on these fields are AMSR-E 89 GHz brightness temperatures (units of K, green, yellow and red) from the 1818 UTC overpass. The pouch sweet spot defined by the intersection of the trough axis (black curve) and critical latitude (CL, purple curve) is highlighted by the black circle. AMSR-E brightness temperature is courtesy of NRL-Monterey.